haematologica
Journal of the Ferrata Storti Foundation

Ligature-induced periodontitis promotes Dnmt3a R878H-driven clonal hematopoiesis

by Qiao Yuan, Min Liao, Ziyao Zhuang, Chenyan Huang, Rixin Chen, Yuxian Song, Yu Wu, Peihui Zou, Lili Li, Hua Nie, Miaomiao Zhang, Shiyuan Song, Yanfen Li and Fuhua Yan

Received: July 28, 2025.
Accepted: December 30, 2025.

Citation: Qiao Yuan, Min Liao, Ziyao Zhuang, Chenyan Huang, Rixin Chen, Yuxian Song, Yu Wu, Peihui Zou, Lili Li, Hua Nie, Miaomiao Zhang, Shiyuan Song, Yanfen Li and Fuhua Yan. Ligature-induced periodontitis promotes Dnmt3a R878H-driven clonal hematopoiesis.
Haematologica. 2026 Jan 22. doi: 10.3324/haematol.2025.288827 [Epub ahead of print]

Ligature-induced periodontitis promotes Dnmt3a R878H-driven clonal hematopoiesis

Qiao Yuan,[1,#], Min Liao,[2,#] Ziyao Zhuang,[1,#] Chenyan Huang,[1] Rixin Chen,[1] Yuxian Song,[1] Yu Wu,[1] Peihui Zou,[3] Lili Li,[1] Hua Nie,[1] Miaomiao Zhang,[1] Shiyuan Song,[1] Yanfen Li,[1,*] Fuhua Yan[1,*]

1. Department of Periodontology, Nanjing Stomatological Hospital, Affiliated Hospital of Medical School, Institute of Stomatology, Nanjing University, Nanjing 210008, China

2. TransThera Sciences (Nanjing), Inc, Nanjing 200120, China

3.Department of Periodontology, Peking University School and Hospital of Stomatology, Peking University, Beijing 100081, China

[#]These authors contributed equally

[*]Corresponding authors

E-mail addresses: liyanfen2003@126.com (Yanfen Li), yanfh@nju.edu.cn (Fuhua Yan)

Running head: Chronic inflammation promotes clonal hematopoiesis

Disclosure

The authors declare no conflict of interest.

Contributions

Fuhua Yan and Yanfen Li: Funding acquisition, Supervision, Project administration. **Qiao Yuan and Min Liao:** Investigation, Methodology, Data curation, Resources, Software, Conceptualization, Writing. **Ziyao Zhuang:** Methodology, Conceptualization, Data curation, Review & editing. **Chenyan Huang and Rixin Chen:** Investigation, Methodology, Formal analysis. **Yuxian Song, Yu Wu, Lili Li,**

Hua Nie, Miaomiao Zhang: Methodology, Formal analysis. **Peihui Zou:** Visualization. **Shiyuan Song:** Methodology.

Acknowledgments

We gratefully acknowledge Dr. Jianwei Wang from Academy of Medical Sciences & Peking Union Medical College for providing the *Dnmt3a*$^{fl\text{-}R878H/+}$ mice.

Funding

This work was supported by the National Key Research and Development Program of China (Grant No. 2023YFC2506300), the Jiangsu Provincial Medical Key Discipline Cultivation Unit (Grant No. JSDW202246), and the High-Level Hospital Construction Project of Nanjing Stomatological Hospital, Affiliated Hospital of Medical School, Institute of Stomatology, Nanjing University (Grant No. 0224C016).

Data Availability Statement

Data are available upon request to the lead contact Fuhua Yan (yanfh@nju.edu.cn). Sequencing data are available at the Gene Expression Omnibus database (http://www.ncbi.nlm.nih.gov/geo/).

Conflict of interest disclosure

The authors declare no conflict of interest.

Data-sharing statement

Data are available upon request to the lead contact Fuhua Yan (yanfh@nju.edu.cn). All sequencing raw data were deposited into the National Center for Biotechnology Information Sequence Read Archive (SRA) with accession number PRJNA1283928.

Word count

Abstract (250 words), main text (4582 words). Including 7 figures and 1 PDF file for all supplementary data.

Abstract

Characterized by somatic mutations (e.g., *DNMT3A*) in blood cells, clonal hematopoiesis (CH) is an age-related process wherein mutated hematopoietic stem and progenitor cells (HSPCs) expand. This expansion thereby increases the risk of all-cause mortality, myeloid hematologic malignancies and other nonmalignant disorders, yet the risk factors that contribute to CH are still largely unknown. Periodontitis induces low-grade systemic inflammation and affects an estimated 62% of dentate adults globally, which may influence CH-associated pathologies. Periodontitis was modeled by bilateral maxillary second molar ligation in mice; CH was established using hematopoietic-specific Dnmt3a R878H mutant mice. Periodontal bone destruction was assessed via micro-computed tomography and H&E-staining. Changes in bone marrow HSPCs, peripheral blood cells, and gingival immune cells were analyzed by flow cytometry. Key molecular mediators were identified through transcriptomic sequencing of sorted gingival myeloid cells and serum cytokine arrays. Results showed that ligature-induced periodontitis (LIP) promoted Dnmt3a R878H-driven clonal hematopoiesis, manifested as a myeloid-biased phenotype characterized by increased myeloid cells in the gingiva and peripheral blood. The selective enrichment of the Dnmt3a R878H clones during LIP is primarily because Dnmt3a R878H HSCs exhibit enhanced resistance and maintain competitive advantages within inflammatory microenvironments. Transcriptomic analysis revealed upregulation of *Ccl17* in gingival R878H myeloid cells, which was corroborated by elevated serum and bone marrow levels of CCL17. The CCL17 upregulation drove myeloid cells recruitment to the gingiva, exacerbating periodontitis while simultaneously reinforcing Dnmt3a R878H HSC expansion. This study highlights the necessity of controlling local chronic inflammation, such as periodontitis, in the clinical management of CH.

Keywords: Dnmt3a R878H; clonal hematopoiesis; hematopoietic stem cells; periodontitis; chemokine

Introduction

Somatic mutations gradually accumulate in normal tissues over time. While the vast majority of these mutations are neutral and not subject to selection, a rare mutation may confer a selective growth advantage on the cell it originates from. This advantage allows the affected cell and its progeny, known as a "clone," to expand progressively. This phenomenon is now recognized to occur in multiple tissues, especially with advanced age. In the context of hematopoietic stem cells (HSCs), it leads to "clonal hematopoiesis" when the mutated clone contributes significantly to the mature blood cell pool.[1-4] While normal hematopoietic stem and progenitor cells (HSPCs) maintain intact self-renewal and regenerative capacities with stable differentiation potential toward both myeloid and lymphoid lineages, those harboring CH-associated mutations exhibit skewed differentiation toward the myeloid compartment.[5] Clonal hematopoiesis (CH) is an emerging condition associated with increased risk of all-cause mortality, myeloid hematologic malignancy, cardiovascular disease and other nonmalignant disorders.[1, 2] Understanding the mechanisms underlying CH could help identify key interventions for this widespread phenomenon, which has significant public health consequences.

CH is an age-related condition that affects 10%–20% of individuals over 70 years of age.[6] However, it has been estimated *DNMT3A* and *TET2* mutations, two most frequent mutations in CH, occur in 95% of individuals aged 50–60.[7] This implies that for most people, acquiring a CH-associated mutation precedes the development of CH itself by decades. Furthermore, *DNMT3A* mutations are known to have minimal impact on steady-state hematopoiesis,[8] indicating environmental factors likely play a major role in triggering CH emergence. Recent studies indicate that common inflammatory conditions, including obesity, diabetes, infections, atherosclerosis, and ulcerative colitis may drive CH pathogenesis.[6, 9-12] In addition, in mouse models, stimulation by microbial signals, TNF-α, and IFN-γ drives the expansion of *DNMT3A*-mutant clones. This occurs because hematopoietic stem cells (HSCs) with

DNMT3A mutations exhibit greater resistance to inflammation-induced depletion than wild-type (WT) HSCs.[5, 9] In this setting, inflammation has been proposed as a key driver that promotes the progress of CH.

Periodontitis involves dysbiosis-driven and low-grade systemic inflammation leading to alveolar bone resorption,[13-16] and is affecting about 62% of dentate adults globally.[17] A study of 4,946 community residents linked *DNMT3A* mutation-driven clonal hematopoiesis to a higher prevalence of periodontal disease. Thus, the authors demonstrate that *DNMT3A* mutation-driven CH exacerbates periodontitis by promoting alveolar bone loss.[18] However, we noticed that the more severe the periodontitis, the higher probability of carrying a *DNMT3A* mutation in the above clinical data. Therefore, we wonder whether periodontitis, as a typical example of chronic inflammation, reciprocally promotes DNMT3A-driven CH.

In this study, we employed a mouse model with hematopoietic-specific expression of the Dnmt3a R878H mutation and a ligature-induced periodontitis (LIP) model to address whether periodontitis promotes Dnmt3a mutation-driven CH, and to elucidate its underlying molecular mechanisms. Our findings demonstrate that periodontitis promotes Dnmt3a R878H-driven CH, as R878H HSCs exhibit enhanced resistance to ligature-induced periodontitis compared with wild-type counterparts, while sustaining competitive advantage and myeloid-biased differentiation under periodontitis. Critically, gingival Dnmt3a R878H myeloid cells exhibit specific upregulation of CCL17, driving a systemic chemokine storm that further fuels CH expansion.

Methods

Mice

Dnmt3a$^{\text{fl-R878H/+}}$ mice were kindly provided by Dr. Jianwei Wang from Academy of Medical Sciences & Peking Union Medical College. CD45.1 mice (Cat. NO. NM-KI-210226) and *Vav1*-cre (Cat. NO. SJ-008610) were purchased from the Shanghai Model Organisms Center, Inc. We crossed *Dnmt3a*$^{\text{fl-R878H/+}}$ mice with Vav1-Cre mice to generate *Dnmt3a*$^{\text{R878H/+}}$ *Vav1*-Cre^{+} mice, which constitutively

express the Cre recombinase and hematopoietic-specific expression of the heterozygous Dnmt3a R878H mutation (referred to as R878H mice). *Dnmt3a*$^{fl\text{-}R878H/+}$ *Vav1*-Cre^{-} and *Dnmt3a*$^{+/+}$ *Vav1*-Cre^{+} (referred to as WT) mice served as bone marrow transplantation (BMT) controls. Recipient mice (CD45.1/2, F1 generated by mating CD45.1 with CD45.2 mice, C57BL/6J background). Mice were housed in individually ventilated cages (IVCs) under specific pathogen-free (SPF) conditions with a standard 12-hour light-dark cycle. Food and water were provided ad libitum. Age-matched mice were used for experiments at 8–10 weeks of age. Data from male and female mice were pooled as no significant sex-based differences were observed. All animal procedures were approved by the Animal Welfare and Ethics Committee of Jiangsu AiLingFei Biotechnology Co., Ltd. (Approval No. JSAB24004M, China) and the Ethical Committee of Nanjing Stomatological Hospital, Medical School of Nanjing University. This study adhered to the ARRIVE (Animal Research: Reporting of *In Vivo* Experiments) guidelines for preclinical animal research.

Ligature-induced periodontitis

Ligature-induced periodontitis mimics human periodontitis by creating a localized biofilm-retentive environment that drives inflammation and bone loss.[19, 20] Briefly, bilateral maxillary second molars were ligated with 4-0 silk sutures. Sutures were checked every other day, and if loosened, teeth were immediately religated. The ligation duration is indicated in the experimental schematic or figure legend. Control mice received sham ligation, where sutures were placed but immediately removed after tying. In some experiments, ligatures were removed after placement to allow inflammation resolution prior to bone marrow (BM) analysis.[21, 22]

Results

Dnmt3a R878H accelerates alveolar bone resorption and infiltration of gingival inflammatory cells

To investigate the biological consequences of periodontitis on Dnmt3a R878H-driven clonal hematopoiesis, *Dnmt3a*$^{fl\text{-}R878H/+}$ mice were crossed with *Vav*-iCre mice to

generate Dnmt3a R878H heterozygous mice (*Dnmt3a*$^{R878H/+}$), in which Dnmt3a R878H is primarily present in hematopoietic cells (hereinafter referred to as R878H mice). *Dnmt3a*$^{+/+}$ littermate mice served as controls (hereinafter named WT mice). Then, R878H and WT mice were subjected to LIP, which is frequently used as an experimental model of periodontitis (*Online Supplementary Figure S1A*).[23] Then, we assessed periodontal destruction via *in vivo* micro-CT, H&E staining, and TRAP staining in mice; inflammatory cell infiltration in gingival tissues was analyzed using flow cytometry (Figure 1A). As expected, significant alveolar bone resorption was observed around the maxillary second molars in both the R878H mutant and WT groups within the ligation group, indicating the successful establishment of ligature-induced periodontitis model. Furthermore, the R878H-LIP group exhibited greater bone resorption compared to the WT-LIP group, indicating Dnmt3a R878H may accelerate alveolar bone resorption under ligation-induced stress (Figure 1B, C; *Online Supplementary Figure S1B*). Histopathological analysis of HE-stained sections revealed common pathological features in LIP groups (WT-LIP and R878H-LIP), including apical migration of the junctional epithelium, epithelial hyperplasia, widened periodontal ligament (PDL) space with collagen fiber disorganization, and dense inflammatory infiltrates. Notably, R878H-LIP mice exhibited mutation-specific aggravation characterized by disruption of epithelial integrity featuring localized ulceration/erosion and intensified inflammation (Figure 1D). TRAP staining of maxillary sections revealed that both genotypes exhibited significantly increased osteoclast numbers around the second molars following LIP induction. In addition, the R878H mutant group demonstrated consistently higher osteoclast counts than the WT group in both ligated and control cohorts (*Online Supplementary Figure S1C*). These results demonstrate Dnmt3a R878H mutation exacerbate periodontal bone destruction.

Additionally, we observed a significantly higher frequency of myeloid cells ($CD45^+CD11b^+$) in gingival tissues of R878H-LIP mice compared to WT-LIP controls (78.5 ± 7.8% *vs*. 45.5 ± 23.8%, $P = 0.01$) (*Online Supplementary Figure S1D*),

suggesting enhanced inflammatory infiltration in R878H-LIP mice. Furthermore, two subsets of myeloid, namely granulocytic myeloid-derived suppressor cells (Gr-MDSC, $CD45^+$ $Ly6C^{low}$ $Ly6G^+$ $CD11b^+$) and monocytic myeloid-derived suppressor cells (Mo-MDSC, $CD45^+$ $Ly6C^+$ $Ly6G^-$ $CD11b^+$), were analyzed (Figure 1E). Compared to WT-LIP controls, the frequency of Mo-MDSCs was significantly increased in R878H-LIP mice (18.8 ± 7.0% *vs.* 7.4 ± 3.9%, $P < 0.001$) (Figure 1F). Although the proportion of Gr-MDSCs was significantly elevated in R878H-LIP mice compared to their untreated controls, no significant difference was observed relative to WT-LIP controls (*Online Supplementary Figure S1E*). These data indicate that the expansion of the myeloid cell pool in R878H-LIP mice is primarily attributable to increased Mo-MDSCs accumulation. In contrast, R878H mice induced by LIP showed a significant decrease in B cell frequency, while WT mice maintained stable B cell populations. There was no significant difference in T cell responses to LIP challenge between R878H mice and WT mice (*Online Supplementary Figure S1F*). Furthermore, the frequency of other myeloid subsets (Ly-$6G^+$ $CD11b^+$, Ly-$6G^-$ $CD11b^+$, and Ly-$6C^-$ Ly-$6G^-$ $CD11b^+$ cells) in gingival tissues exhibited no significant difference between LIP-challenged WT/R878H mice and their untreated controls *Online Supplementary Figure S1G*). These observations with regard to the upregulation of infiltration of inflammatory cells as well as myeloid-biased phenotype were remarkably similar to a recent report.[18]

Ligature-induced periodontitis promotes Dnmt3a R878H-driven clonal hematopoiesis via a myeloid-biased phenotype

Chronic inflammation at a local site is an established driver of secondary pathologies in distal organs. Within the BM, HSPCs function as key responders to systemic inflammatory signals, undergoing expansion and directing the differentiation of myeloid lineage cells.[24-26] While the data above revealed that periodontitis induces a myeloid-skewed phenotype in mice harboring Dnmt3a-mutant HSPCs, our subsequent objective was to determine if periodontitis promotes R878H-driven clonal

hematopoiesis. To assess clonal expansion, we employed a competitive bone marrow transplantation (BMT) assay, following established methodologies.[5, 6] 1×10^5 freshly isolated total bone marrow cells from either WT or R878H mice were transplanted into lethally irradiated recipients together with 5×10^5 competitor cells. One month post-transplantation, half of recipient mice per experimental group were maintained under LIP conditions until study termination. Subsequently, alveolar bone loss was quantified by *in vivo* micro-CT one month after LIP induction and peripheral blood chimerism was monitored monthly (Figure 2A). R878H cells demonstrated a significant competitive advantage over competitor cells following LIP challenge compared to untreated controls (40.9 ± 15.8% *vs.* 20.4 ± 10.9%, $P = 0.04$), and the difference primarily attributable to the myeloid lineage (Figure 2B, C; *Online Supplementary Figure S2A–C*). The mature hematopoietic lineage distribution of R878H cells was comparable between the R878H-LIP and R878H-CTL groups (*Online Supplementary Figure S2D, E*). In addition, both the reconstitution capacity and lineage distribution of WT cells were unaffected by LIP challenge, showing no significant difference between the LIP and control groups (Figure 2B, C; *Online Supplementary Figure S2C–E*). Five months post-transplantation, donor-derived HSPCs in BM of recipient mice were analyzed (Figure 2D). The results revealed both donor-derived R878H HSCs, myeloid progenitors, LSK were significantly increased upon LIP challenge compared to untreated controls. This effect was specific to the R878H group, with no significant differences observed in donor-derived in WT mice (Figure 2E; *Online Supplementary Figure S2F, G*). Analysis of donor-derived lineage cells within the gingiva of recipient mice revealed significantly greater infiltration of donor-derived myeloid cells, but not B cells and T cells, in the R878H-LIP group compared to all other groups (*Online Supplementary Figure S2H*), indicating exacerbated gingival tissue injury in R878H-LIP recipients. Collectively, these findings suggest that LIP promotes Dnmt3a R878H-driven clonal hematopoiesis by facilitating the recruitment and infiltration of myeloid cells into the gingiva tissues. Presumably, these localized chronic inflammatory processes may subsequently

accelerate clonal hematopoiesis through direct or indirect mechanisms.

R878H HSCs exhibit greater resistance to inflammation induced by periodontitis than WT HSCs

CH is characterized by the disproportionate contribution of expanded HSPC clones to blood cell production, which occurs because these clones exhibit greater resistance to inflammation-induced damage than WT cells.[5, 27-29] Previous work established that the Dnmt3a R878H mutation confers LPS greater resistance in HSCs than WT.[5] To determine if this phenotype extends to LIP, R878H and WT mice were subjected to LIP. Three weeks later, lineage cells in the PB and HSPCs in the BM were analyzed by flow cytometry (Figure 3A). Compared to WT, Dnmt3a R878H mice showed increased long-term HSCs (LT-HSCs) frequency (0.0293 ± 0.0086% *vs*. 0.0103 ± 0.0043%, $P < 0.001$) and absolute number (7.98×10^3 vs 2.65×10^3 cells/femur, $P < 0.001$) (Figure 3B, C; *Online Supplementary Figure S3A*), which is consistent with previous report that Dnmt3a R878H mutation leads to expansion of HSC pool.[30, 31] In WT mice subjected to LIP, the frequency and absolute number of LT-HSCs, short-term HSCs (ST-HSCs), megakaryocyte-erythroid progenitors (MEP), and common myeloid progenitors (CMP) significantly decreased. In contrast, these populations remained unchanged in R878H mice upon LIP-induced inflammatory challenge (Figure 3C, D; *Online Supplementary Figure S3A–C*), indicating R878H cells exhibit diminished responsiveness to inflammatory stimulation. Whereas R878H and WT multipotent progenitors (MPPs) exhibited no difference in response to LIP stimulation (Figure 3E), but both WT and R878H mice showed a significant expansion of granulocyte-macrophage progenitors (GMPs) following LIP treatment compared to untreated controls (Figure 3F; *Online Supplementary Figure S3D*). This aligns with prior studies demonstrating that chronic LIP-driven sustained myelopoietic enhancement.[23] Furthermore, the frequencies of lineage cells (including B cells, T cells, and myeloid cells) (*Online Supplementary Figure S3E*) and specific myeloid subsets ($Ly6G^+$ $CD11b^+$, $Ly6G^-$ $CD11b^+$, Gr-MDSC and Mo-MDSC) (*Online*

Supplementary Figure S3F) in the PB, and immune cells (B cells, T cells, and myeloid cells) in the BM (*Online Supplementary Figure S3G*), did not differ between LIP-challenged WT/R878H mice and their corresponding untreated controls. These data demonstrate that the Dnmt3a R878H mutation confers greater resistance to inflammatory challenge in HSCs and specific myeloid progenitor populations compared to WT counterpart following LIP.

LIP-stressed R878H HSCs maintain a competitive advantage and a myeloid-biases differentiation

Clonal hematopoiesis results from somatic mutations that confer a competitive advantage to blood stem/progenitor cells under selective pressures like inflammation or chemotherapy.[28, 30, 32, 33] Given that periodontitis is a chronic systemic inflammatory disease, we hypothesize that it may promote Dnmt3a R878H-driven clonal hematopoiesis through mechanisms similar to those observed with canonical inflammatory stimuli (e.g., LPS or cytokine exposure).[9, 34] To test this hypothesis, a total of 5×10^5 bone marrow cells isolated from either LIP/CTL-treated R878H or LIP/CTL-treated WT mice were transplanted into lethally irradiated recipient mice, along with 5×10^5 competitor cells. Peripheral blood chimerism was subsequently monitored monthly until the fourth month post-transplantation (Figure 4A). The result shows that the chronic LIP challenged R878H cells significantly outcompeted the competitor cells compared to untreated controls (76.5 ± 8.6% *vs.* 67.3 ± 8.5%, P = 0.04) and the difference mainly stemmed from the B cells and myeloid lineage (Figure 4B; *Online Supplementary Figure S4A*). In contrast, there was no difference between LIP-treated and CTL-treated WT cells (Figure 4C; *Online Supplementary Figure S4B*). Notably, the myeloid-skewed differentiation in recipients of periodontitis-exposed donor cells reinforces the concept of a transplantable maladaptive trained myelopoiesis phenotype driven by experimental periodontitis (Figure 4D).[23]

To investigate whether donor-derived HSCs in LIP-treated R878H cells in recipient

mice acquire a proliferative advantage over their untreated counterparts, as observed in peripheral blood cells, we analyzed donor-derived HSCs at 4 months post-transplantation (Figure 4E). We observed that donor-derived HSCs were increased significantly upon LIP challenge in the R878H group compared with untreated controls (94.2 ± 3.3% *vs.* 82.5 ± 2.7%, $P < 0.001$) (Figure 4F). Meanwhile, donor-derived myeloid progenitors (*Online Supplementary Figure S4C*), lineage negative cells (*Online Supplementary Figure S4D*) and progenitor cells (LSK) (*Online Supplementary Figure S4E*) exhibited the same trend as HSCs. However, this trend was not observed in the WT group. Collectively, these data suggest that LIP stress enhanced the functional capacity of R878H HSCs and lead to a myeloid-biases differentiation of mutant HSCs, which may explain why R878H cells can be selected under LIP challenge and increase myeloid cells infiltration in gingival tissue.

Activation of chemokine signaling in Dnmt3a R878H mutant myeloid cells in gingiva under periodontitis

To investigate the mechanisms by which myeloid cells harboring the *Dnmt3a* R878H mutation exacerbate both periodontitis and clonal hematopoiesis, we performed transcriptome analysis on gingival $CD45.2^+$ $CD11b^+$ cells isolated from recipient mice in Figure 2A. Compared to control mice, we identified 585 differentially expressed genes (DEGs) in donor-derived myeloid cells from LIP-subjected WT recipient mice, with 281 significantly upregulated and 304 significantly downregulated ($P < 0.05$). Similarly, 527 DEGs were identified in donor-derived myeloid cells from LIP-subjected R878H recipient mice versus controls, comprising 253 upregulated and 274 downregulated genes ($P < 0.05$) (*Online Supplementary Figure S5A, B*). Analysis of genes significantly upregulated in the R878H-LIP group compared to all three other groups revealed 34 genes specifically upregulated in R878H-LIP cells (*Online Supplementary Figure S5C*). Excluding genes with unknown function, the gene set specifically upregulated in R878H-LIP cells was enriched for chemokine-related genes, including *Ccl22*, *Ccl4*, *Ccl17*, *Cx3cr1*, and *Cxcr1* (Figure 5A). Gene Ontology

(GO) enrichment analysis demonstrated that terms including "chemokine-mediated signaling pathway", "cell-cell adhesion", "lymphocyte chemotaxis", "monocyte chemotaxis", "CCR chemokine receptor binding", and "chemokine activity" were significantly overrepresented among the upregulated genes in the R878H-LIP group compared to the R878H-CTL group (Figure 5B). In contrast, these terms were not enriched in the WT-LIP group relative to the WT-CTL group (Figure 5C). Furthermore, the GO term "cytokine receptor activity" was enriched in both the R878H-LIP and WT-LIP groups, suggesting that cytokines such as interleukins may respond to LIP-induced inflammation in both R878H and WT cells. Consistent with the specific enrichment of chemotaxis genes in LIP-exposed R878H cells, gene set enrichment analysis (GSEA) revealed significant enrichment of chemokine activity target genes in LIP-stimulated R878H cells (normalized enrichment score (NES) = 1.58; false-discovery rate (FDR)-adjusted q = 0.033), but not in WT-LIP cells (NES = 0.77; FDR-adjusted q = 0.76) (Figure 5D). Despite a previous report of their downregulation in R878H cells,[34] necroptosis activation-related genes were not enriched in either WT or R878H mice after LIP compared to the control group (*Online Supplementary Figure S5D*). These findings indicate that *Dnmt3a* R878H mutant myeloid cells in gingiva are primed to activate transcriptional programs associated with chemotaxis following LIP exposure.

To validate these findings, we quantified chemokine expression in recipient mouse gingival tissue using quantitative real-time polymerase chain reaction (qPCR) (Figure 5E). Results confirmed that *Ccl22*, *Ccl4*, *Ccl17*, *Cx3cr1*, and *Cxcr1* were specifically upregulated in the gingiva of the R878H-LIP group, aligning with the transcriptomic data (Figure 5F, *Online Supplementary Figure S5F*). Additionally, *Ccr5* (receptor for *Ccl4*) and *Cx3cl1* (ligand for *Cx3cr1*) were upregulated in R878H-LIP cells (*Online Supplementary Figure S5E*). Other chemokines (*Ccl5*, *Ccl9*, *Ccl20*, *Cxcl11*) were also elevated in the gingiva of R878H-LIP mice (*Online Supplementary Figure S5E, G*). Furthermore, qPCR confirmed enrichment of two previously reported cytokines (*Tnf* and *Il1β*) in the R878H-LIP group (*Online Supplementary Figure S5H*).[18] A

recent report identified ALPK1 as a critical receptor mediating ADP-heptose–induced expansion of *Dnmt3a* R878H HSCs by triggering TIFAsome assembly, NF-κB activation, and pro-survival transcriptional reprogramming, conferring a competitive advantage over WT HSCs.[33] Consistent with this, we observed upregulation of *Alpk1* in the R878H-LIP group in both transcriptomic data and qPCR results (*Online Supplementary Table S2, Figure S5I*). The data above indicate the chemokine signaling was specifically upregulated in gingival myeloid cells of R878H mice under LIP challenge.

Dnmt3a R878H drives systemic chemokine storm in periodontitis-associated clonal hematopoiesis

Given that R878H-mutant myeloid cells exacerbate periodontitis via specific chemokine secretion upon LIP stimulation, we hypothesized that these secreted chemokines might enter systemic circulation, potentially promoting clonal hematopoiesis by acting directly or indirectly upon HSPCs in the bone marrow. To test this, we performed cytokine array assays on serum of recipient mice in Figure 2A. Results identified 82 proteins specifically upregulated in the R878H-LIP group compared to all three other groups, including 17 chemokines, 10 interleukins, 9 TNF superfamily members, 9 growth factors, 3 adhesion molecules, and 44 other proteins (Figure 6A; *Online Supplementary Figure S6A, Table S3*). Notably, CCL4 and CCL17, upregulated in R878H-LIP myeloid cells, were also elevated in the serum of R878H-LIP recipients (Figure 6B). CCL4 is a recognized proinflammatory gene in monocytes from *DNMT3A* mutation carriers with heart failure.[35] Furthermore, consistent with a prior report that *Dnmt3a* inactivation enhances *Ccl5* expression in LPS-stimulated macrophages, *Ccl5* levels were upregulated in R878H-LIP cells, although increases in *Cxcl1* and *Cxcl2* were not observed in our assays.[36] GO enrichment analysis showed significant overrepresentation of terms including "neutrophil chemotaxis", "chemotaxis", "chemokine-mediated signaling pathway", "monocyte chemotaxis", "lymphocyte chemotaxis", "CCR chemokine receptor

binding", "chemokine activity", "CXCR chemokine receptor binding", and "chemokine receptor binding" among the upregulated genes in the R878H-LIP group versus R878H-CTL (Figure 6C), while these terms were not enriched in the WT-LIP group compared to WT-CTL (Figure 6D).

To further confirm these results, we measured serum chemokine levels using enzyme-linked immunosorbent assays (ELISA) (Figure 6E). Consistent with the cytokine array data, proteins including CCL4, CCL17, PF4, CXCL11, CXCL5, CXCL12, CXCL16 and CX3CL1 were specifically increased in the serum of R878H-LIP recipients, whereas CXCL1 was conversely reduced (Figure 6F; *Online Supplementary Figure S6B*). Furthermore, we observed elevated serum levels of CCL5, CCL11, TNFSF11 (RANKL receptor), TNFRSF11B, IL17β, and IL22 in R878H-LIP recipients (*Online Supplementary Figure S6C, D*). Chemokine levels in the bone marrow of recipient mice were measured by ELISA. The results revealed a specific increase in CCL17 in the bone marrow of R878H-LIP recipients; however, CCL4 was not detected in any recipient group (*Online Supplementary Figure S6E*).

CCL17 expands R878H HSCs *in vitro*

To determine if the specific elevation of CCL4 and CCL17 in gingival myeloid cells and serum directly promotes CH by driving HSC proliferation, we treated freshly isolated WT and R878H HSCs with these chemokines (Figure 7A). The results showed that neither CCL4 nor CCL17 affected the colony size and total cell number of either genotype after 6 days (Figure 7B; *Online Supplementary Figure S7A*). However, flow cytometric analysis of phenotypic HSCs ($CD150^+$ $CD48^-$ $SCA\text{-}1^+$ $c\text{-}KIT^+$) demonstrated a specific ~50% increase in the number and frequency of R878H HSCs upon CCL17 treatment compared to WT controls, an effect not seen with CCL4 (Figure 7C; *Online Supplementary Figure S7B*). Thus, CCL17 selectively promotes the expansion of R878H HSCs.

Combined with our transcriptomic and protein data, these results suggest that periodontitis specifically upregulates CCL17 in the context of the R878H mutation,

potentially establishing a vicious cycle wherein CCL17 mediates the crosstalk between Dnmt3a R878H-driven CH and periodontitis (Figure 7D).

Discussion

In this study, we report for the first time that ligature-induced periodontitis promotes Dnmt3a R878H-driven clonal hematopoiesis. We demonstrate that LIP acts as a potent inflammatory stressor promoting the selective expansion of Dnmt3a R878H-mutant HSPCs in transplantation models. Crucially, this expansion is not merely a passive consequence of inflammation but actively fuels a vicious cycle: R878H-mutant myeloid cells exhibit a hyper-inflammatory phenotype within the gingiva, characterized by specific chemokine hyper-secretion, which exacerbates periodontal bone destruction and creates a systemic chemokine storm. This storm, we posit, further stimulates the bone marrow niche, amplifying *Dnmt3a* mutant HSC clonal advantage. Our findings position periodontitis, a highly prevalent chronic inflammatory disease, as a significant driver and amplifier of *Dnmt3a*-mutant CH, with profound implications for understanding CH progression and its associated comorbidities.

The observation that LIP selectively enhances the competitive fitness of Dnmt3a R878H HSPCs over WT cells in transplantation assays (Figure 2B–C) provides direct experimental evidence supporting periodontitis as a driver of CH, extending beyond classical stressors like aging or chemotherapy.[2, 3, 30] This could be due to either LIP enhancing the functionality of R878H HSCs, or alternatively, R878H HSCs exhibiting resistance to inflammatory stimuli within the bone marrow microenvironment of irradiated recipient mice under transplantation stress, thereby selectively depleting WT HSCs and consequently increasing the ratio of R878H HSCs. A recent study may provide supports for the latter hypothesis.[32] It has been established that chronic inflammation provides a selective pressure favoring mutant HSPCs bearing mutations in genes like *DNMT3A* and *TET2*.[5, 9, 28] Our data extend this concept to the oral cavity, demonstrating that localized periodontal inflammation, mirroring human disease, is

sufficient to trigger and sustain mutant clonal expansion. Based on the findings of Agarwal et al.[33], ADP-heptose, a microbiota-derived metabolite enriched in aging, binds to ALPK1 on DNMT3A R878H-mutant HSCs, triggering TIFAsome formation, NF-κB activation, and transcriptional reprogramming that confers a selective competitive advantage and drives clonal expansion. Periodontitis is characterized by dysbiosis dominated by Gram-negative bacteria (e.g., *Porphyromonas gingivalis*), barrier dysfunction, and systemic inflammation. Future studies should evaluate whether periodontal disease-associated dysbiosis and mucosal barrier disruption elevate circulating ADP-heptose, thereby activating the ALPK1-NF-κB axis in HSPCs to promote clonal expansion in individuals with *DNMT3A* mutations.

Furthermore, our findings reveal that R878H HSCs resist LIP-induced depletion (Figure 3C), aligning with known LPS hyporesponsiveness in *Dnmt3a*-mutant HSCs.[5] This adaptation likely underpins clonal persistence during inflammation. Furthermore, the R878H mutation not only exacerbates periodontal bone loss by enhancing myeloid cell infiltration—particularly Mo-MDSCs—but also confers resistance to inflammatory damage in HSPCs (Figure 1F and 3C). This aligns with clinical studies showing *DNMT3A* mutations correlate with heightened inflammation in cardiovascular tissues.[36] The myeloid skewing in LIP-treated mice mirrors "trained myelopoiesis" observed in chronic inflammation,[23] suggesting epigenetic reprogramming enables maladaptive myeloid responses.

The core mechanistic insight lies in the establishment of a chemokine-driven feedback loop. Transcriptomic profiling of gingival myeloid cells isolated from recipient mice revealed a unique signature in the R878H-LIP group: specific upregulation of chemokines (*Ccl4*, *Ccl17*, *Ccl22*) and enrichment of chemokine signaling pathways. This R878H-specific chemokine activation program was absent in WT-LIP myeloid cells (Figure 5F). Critically, this local chemokine storm translated systemically. Cytokine array and ELISA analysis of recipient serum identified a constellation of chemokines (CCL4, CCL17) specifically elevated in the serum of R878H-LIP recipients (Figure 6F). These chemokines, particularly CCL17, previously implicated

in regulating hematopoietic stem/ progenitor cell migration and retention in mouse fetal liver[36]—likely drives the pathogenic cycle through dual mechanisms: (1) Local tissue destruction: enhanced recruitment of Mo-MDSCs and other myeloid effectors into the gingiva, directly amplifying osteoclastogenesis and bone resorption; (2) Systemic clonal selection: creation of a chemokine gradient that selectively promotes the survival, proliferation, or bone marrow homing of R878H HSPCs. Our transplantation data support this, showing LIP exposure specifically boosted R878H (but not WT) myeloid progenitor engraftment. This establishes chemokines not merely as inflammatory markers but as mediators bridging peripheral inflammation to stem cell fitness. This chemokine-associated vicious cycle represents a novel mechanism distinct from the IL-1β-centric maladaptive myelopoiesis described by Li et al.,[23] highlighting the mutation-specific rewiring of inflammatory pathways.

The chemokine storm, originating from the inflamed periodontium populated by hyper-secretory mutant myeloid cells, is hypothesized to act back on the bone marrow. Chemokines like CCL4, CCL5, and CXCL12 are potent regulators of HSC proliferation, differentiation, and migration.[37, 38] Their systemic elevation likely directly or indirectly (e.g., via niche modulation) provides a sustained pro-proliferative and pro-survival signal specifically advantageous to R878H HSPCs, explaining their enhanced repopulating advantage after LIP exposure. This establishes a self-reinforcing loop: Periodontitis -> Mutant myeloid expansion/infiltration -> Local chemokine hyper-secretion -> Systemic chemokine storm -> Enhanced mutant HSC expansion/clonal hematopoiesis -> More mutant myeloid cells -> Aggravated periodontitis (Figure 7D).

Our findings have significant clinical implications. They position periodontitis not only as a consequence of systemic inflammation linked to CH, but as an active driver of *DNMT3A*-mutant clonal expansion. This suggests that effective periodontal therapy could be crucial for mitigating the progression of clonal hematopoiesis in individuals harboring *DNMT3A* mutations. Furthermore, the identified chemokine signature (e.g., CCL17) in both gingival tissue and serum of R878H-LIP mice presents potential

biomarkers for monitoring this pathogenic interaction or therapeutic targets. Interventions aimed at disrupting specific chemokine axes (e.g., CCR4 for CCL17) could potentially break this deleterious feedback loop, offering a novel strategy to manage both periodontitis severity and CH progression in mutation carriers. However, other chemical therapies (rapamycin, metformin and oridonin) may also suppresses *DNMT3A* mutation-driven clonal hematopoiesis and alveolar bone loss.[18, 34, 39-41] Furthermore, our study suggests that periodontitis may establish a link with low-grade systemic inflammation via hematogenous routes, offering novel perspectives for future research on periodontal-systemic disease connections.

Important questions remain. Does Dnmt3a R878H alter chemokine receptor expression on HSPCs, enhancing their responsiveness? Do chemokines like CCL17 directly stimulate R878H HSC self-renewal? How does R878H specifically prime chemokine genes? Does periodontitis promote other CHIP mutations (e.g., TET2)? Furthermore, while we focused on myeloid cells, the observed expansion within the B-cell lineage in some transplantation settings warrants investigation into potential B-cell intrinsic effects of the mutation in the context of inflammation. The duration of this chemokine-mediated priming and its dependence on continuous inflammatory stimuli also need exploration.

References

1. Genovese G, Kahler AK, Handsaker RE, et al. Clonal hematopoiesis and blood-cancer risk inferred from blood DNA sequence. N Engl J Med. 2014;371(26):2477-2487.
2. Jaiswal S, Ebert BL. Clonal hematopoiesis in human aging and disease. Science. 2019;366(6465):eaan4673.
3. Jaiswal S, Fontanillas P, Flannick J, et al. Age-related clonal hematopoiesis associated with adverse outcomes. N Engl J Med. 2014;371(26):2488-2498.
4. Jaiswal S, Natarajan P, Silver AJ, et al. Clonal Hematopoiesis and Risk of Atherosclerotic Cardiovascular Disease. N Engl J Med. 2017;377(2):111-121.
5. Liao M, Chen R, Yang Y, et al. Aging-elevated inflammation promotes DNMT3A R878H-driven clonal hematopoiesis. Acta Pharm Sin B. 2022;12(2):678-691.
6. Pasupuleti SK, Ramdas B, Burns SS, et al. Obesity-induced inflammation exacerbates clonal hematopoiesis. J Clin Invest. 2023;133(11):e163968.
7. Young AL, Challen GA, Birmann BM, Druley TE. Clonal haematopoiesis harbouring AML-associated mutations is ubiquitous in healthy adults. Nat Commun. 2016;7:12484.
8. Buscarlet M, Provost S, Zada YF, et al. DNMT3A and TET2 dominate clonal hematopoiesis and demonstrate benign phenotypes and different genetic predispositions. Blood. 2017;130(6):753-762.
9. Hormaechea-Agulla D, Matatall KA, Le DT, et al. Chronic infection drives Dnmt3a-loss-of-function clonal hematopoiesis via IFNgamma signaling. Cell Stem Cell. 2021;28(8):1428-1442.
10. Tobias DK, Manning AK, Wessel J, et al. Clonal Hematopoiesis of Indeterminate Potential (CHIP) and Incident Type 2 Diabetes Risk. Diabetes Care. 2023;46(11):1978-1985.
11. Oren O, Small AM, Libby P. Clonal hematopoiesis and atherosclerosis. J Clin Invest. 2024;134(19):e180066.
12. Esai Selvan M, Nathan DI, Guisado D, et al. Clonal hematopoiesis of

indeterminate potential in crohn's disease and ulcerative colitis. Inflamm Bowel Dis. 2025;31(8):2123-2133.

13. Lamont RJ, Koo H, Hajishengallis G. The oral microbiota: dynamic communities and host interactions. Nat Rev Microbiol. 2018;16(12):745-759.
14. Bao J, Li L, Zhang Y, et al. Periodontitis may induce gut microbiota dysbiosis via salivary microbiota. Int J Oral Sci. 2022;14(1):32.
15. Hu W, Chen S, Zou X, et al. Oral microbiome, periodontal disease and systemic bone-related diseases in the era of homeostatic medicine. J Adv Res. 2025;73:443-458.
16. Chen BY, Lin WZ, Li YL, et al. Roles of oral microbiota and oral-gut microbial transmission in hypertension. J Adv Res. 2023;43:147-161.
17. Trindade D, Carvalho R, Machado V, Chambrone L, Mendes JJ, Botelho J. Prevalence of periodontitis in dentate people between 2011 and 2020: A systematic review and meta-analysis of epidemiological studies. J Clin Periodontol. 2023;50(5):604-626.
18. Wang H, Divaris K, Pan B, et al. Clonal hematopoiesis driven by mutated DNMT3A promotes inflammatory bone loss. Cell. 2024;187(14):3690-3711.
19. Abe T, Hajishengallis G. Optimization of the ligature-induced periodontitis model in mice. J Immunol Methods. 2013;394(1-2):49-54.
20. Kitamoto S, Nagao-Kitamoto H, Jiao Y, et al. The Intermucosal Connection between the Mouth and Gut in Commensal Pathobiont-Driven Colitis. Cell. 2020;182(2):447-462.
21. Kourtzelis I, Li X, Mitroulis I, et al. DEL-1 promotes macrophage efferocytosis and clearance of inflammation. Nat Immunol. 2019;20(1):40-49.
22. Li X, Colamatteo A, Kalafati L, et al. The DEL-1/β3 integrin axis promotes regulatory T cell responses during inflammation resolution. J Clin Invest. 2020;130(12):6261-6277.
23. Li X, Wang H, Yu X, et al. Maladaptive innate immune training of myelopoiesis links inflammatory comorbidities. Cell. 2022;185(10):1709-1727.

24. Essers MA, Offner S, Blanco-Bose WE, et al. IFNalpha activates dormant haematopoietic stem cells in vivo. Nature. 2009;458(7240):904-908.
25. Matatall KA, Jeong M, Chen S, et al. Chronic Infection Depletes Hematopoietic Stem Cells through Stress-Induced Terminal Differentiation. Cell Rep. 2016;17(10):2584-2595.
26. Zhao JL, Ma C, O'Connell RèM, et al. Conversion of Danger Signals into Cytokine Signals by Hematopoietic Stem and Progenitor Cells for Regulation of Stress-Induced Hematopoiesis. Cell Stem Cell. 2014;14(4):445-459.
27. Abegunde SO, Buckstein R, Wells RA, Rauh MJ. An inflammatory environment containing TNFα favors Tet2-mutant clonal hematopoiesis. Exp Hematol. 2018;59:60-65.
28. Cai Z, Kotzin JJ, Ramdas B, et al. Inhibition of Inflammatory Signaling in Tet2 Mutant Preleukemic Cells Mitigates Stress-Induced Abnormalities and Clonal Hematopoiesis. Cell Stem Cell. 2018;23(6):833-849.
29. Meisel M, Hinterleitner R, Pacis A, et al. Microbial signals drive pre-leukaemic myeloproliferation in a Tet2-deficient host. Nature. 2018;557(7706):580-584.
30. Guryanova OA, Shank K, Spitzer B, et al. DNMT3A mutations promote anthracycline resistance in acute myeloid leukemia via impaired nucleosome remodeling. Nat Med. 2016;22(12):1488-1495.
31. Loberg MA, Bell RK, Goodwin LO, et al. Sequentially inducible mouse models reveal that Npm1 mutation causes malignant transformation of Dnmt3a-mutant clonal hematopoiesis. Leukemia. 2019;33(7):1635-1649.
32. Jakobsen NA, Turkalj S, Zeng AGX, et al. Selective advantage of mutant stem cells in human clonal hematopoiesis is associated with attenuated response to inflammation and aging. Cell Stem Cell. 2024;31(8):1127-1144.
33. Agarwal P, Sampson A, Hueneman K, et al. Microbial metabolite drives ageing-related clonal haematopoiesis via ALPK1. Nature. 2025;642(8066):201-211.
34. Liao M, Dong Q, Chen R, et al. Oridonin inhibits DNMT3A R882

mutation-driven clonal hematopoiesis and leukemia by inducing apoptosis and necroptosis. Cell Death Discov. 2021;7(1):297.

35. Abplanalp WT, Cremer S, John D, et al. Clonal Hematopoiesis-Driver DNMT3A Mutations Alter Immune Cells in Heart Failure. Circ Res. 2021;128(2):216-228.
36. Konno K, Sasaki T, Kulkeaw K, Sugiyama D. Paracrine CCL17 and CCL22 signaling regulates hematopoietic stem/progenitor cell migration and retention in mouse fetal liver. Biochem Bioph Res Co. 2020;527(3):730-736.
37. Ergen AV, Boles NC, Goodell MA. Rantes/Ccl5 influences hematopoietic stem cell subtypes and causes myeloid skewing. Blood. 2012;119(11):2500-2509.
38. Nakatani T, Sugiyama T, Omatsu Y, Watanabe H, Kondoh G, Nagasawa T. Ebf3(+) niche-derived CXCL12 is required for the localization and maintenance of hematopoietic stem cells. Nat Commun. 2023;14(1):6402.
39. Gozdecka M, Dudek M, Wen S, et al. Mitochondrial metabolism sustains DNMT3A-R882-mutant clonal haematopoiesis. Nature. 2025;642(8067):431-441.
40. Hosseini M, Voisin V, Chegini A, et al. Metformin reduces the competitive advantage of Dnmt3a(R878H) HSPCs. Nature. 2025;642(8067):421-430.
41. Young KA, Hosseini M, Mistry JJ, et al. Elevated mitochondrial membrane potential is a therapeutic vulnerability in Dnmt3a-mutant clonal hematopoiesis. Nat Commun. 2025;16(1):3306.

Figure 1 Dnmt3a R878H accelerates alveolar bone resorption and infiltration of gingival inflammatory cells

(A-F) Periodontal destruction and gingival tissues from R878H and WT mice were assessed following 21-day ligature-induced periodontitis (LIP) or sham control (CTL). (A) Experimental design. (B) Micro-CT quantification of alveolar bone resorption (CEJ-ABC distance), cementoenamel junction (CEJ), alveolar bone crest (ABC). (C) Site-specific CEJ-ABC measurements (mesial) of maxillary left second molars across groups. (D) H&E staining revealing histological alterations in gingival epithelium, periodontal ligament interface, and connective tissue. (E) Representative FACS plots to identify myeloid cells ($CD45^+$ $CD11b^+$), Mo-MDSC ($CD45^+$ $Ly6C^+$ $Ly6G^-$ $CD11b^+$) and Gr-MDSC ($CD45^+$ $Ly6C^-$ $Ly6G^+$ $CD11b^+$) in the gingiva of mice in LIP/CTL groups. (F) The frequency of Mo-MDSCs population in gingival tissues. n = 4–5 mice (2–3 months) per group from two independent experiments. All data above are shown as mean ± SEM and were analyzed using a two-way ANOVA followed by Sidak's multiple comparisons test.

Figure 2 Ligature-induced periodontitis promotes Dnmt3a R878H-driven clonal hematopoiesis via a myeloid-biased phenotype

(A–E) Freshly isolated BM cells (1×10^5, CD45.2) from 2-month-old R878H mice or age-matched WT mice were transplanted into lethally irradiated recipients (CD45.1/2) alongside 5×10^5 competitor cells (CD45.1). One month post-transplantation, recipient mice underwent either LIP or sham procedures (CTL). Chimera in the peripheral blood was assessed monthly for five months. (A) Experimental design. (B–C) Donor-derived ($CD45.2^+$) contribution to overall cells (B) and myeloid cells ($CD11b^+$) (C) from R878H (red) and WT (black) mice. (D) Representative FACS plots identifying donor-derived HSC ($CD34^-$ LSK) cells in the bone marrow of recipients at the fifth month after transplantation. (E) The histograms show the percentage of WT/R878H-derived ($CD45.2^+$) HSCs in LIP group (red) and CTL

group (black). *n* = 4–6 mice per group from two independent experiments. All data above are shown as mean ± SEM and were analyzed using a two-way ANOVA followed by Sidak's multiple comparisons test.

Figure 3 R878H HSCs exhibit greater resistance to inflammation induced by periodontitis than WT HSCs

(A–F) 2–3 months old R878H and age-matched WT mice received 21-day exposure to LIP or sham control (CTL), and hematopoietic stem/progenitor cells (HSPCs) in bone marrow (BM) and lineage cells in peripheral blood (PB) of mice were analyzed by fluorescence-activated cell sorting (FACS). (A) Experimental design. (B) Representative FACS plots depict the gating strategies for LSK (lineage$^-$ Sca-1$^+$ c-kit$^+$), LK (lineage$^-$ Sca-1$^-$ c-kit$^+$), LT-HSC (lineage$^-$ Sca-1$^+$ c-kit$^+$ CD135$^-$ CD34$^-$), ST-HSC (lineage$^-$ Sca-1$^+$ c-kit$^+$ CD135$^-$ CD34$^+$), MPP (lineage$^-$ Sca-1$^+$ c-kit$^+$ CD135$^+$ CD34$^+$), CMP (lineage$^-$ Sca-1$^-$ c-kit$^+$ CD16/32$^-$ CD34$^+$), GMP (lineage$^-$ Sca-1$^-$ c-kit$^+$ CD16/32$^+$ CD34$^+$) and MEP (lineage$^-$ Sca-1$^-$ c-kit$^+$ CD16/32$^-$ CD34$^-$) cells analysis in the BM of WT and R878H mice treated with or without LIP. (C-F) Histograms showing the frequency of long-term hematopoietic stem cells (LT-HSCs) (C), short-term hematopoietic stem cells (ST-HSCs) (D), multipotent progenitors (MPPs) (E) and granulocyte-macrophage progenitors (GMPs) (F) in the bone marrow of WT and R878H mice treated with or without LIP. *n* = 4–5 mice per group from two independent experiments. All data above are shown as mean ± SEM and were analyzed using a two-way ANOVA followed by Sidak's multiple comparisons test.

Figure 4 LIP-stressed R878H HSCs maintain a competitive advantage and a myeloid-biases differentiation

(A–F) 2-month-old R878H (CD45.2$^+$) and WT (CD45.2$^+$) mice underwent LIP or sham operations for 21 days (n = 6/group), establishing four experimental cohorts.

BM cells (CD45.2) were isolated from mice of each group and transplanted (5×10^5 cells/mouse) alongside 5×10^5 competitor BM cells (CD45.1) into lethally irradiated young recipient mice (CD45.1/2, 2-3 months old). Peripheral blood chimerism was monitored monthly for 4 months post-transplantation. (A) Experimental design. (B–C) Donor-derived ($CD45.2^+$) contribution to overall cells from R878H (B) and WT (C) recipient mice subjected, or not (control), to LIP. (D) Lineage distribution of B cells, myeloid cells and T cells among donor-derived cells in the PB of recipients carrying R878H or WT BM cells treated with or without LIP at the 4^{th} month after transplantation. (E) Representative flow cytometry plots exhibit the gating strategy and the frequency of donor-derived HSC ($CD34^-$ LSK) in the indicated recipients at the fourth month after transplantation. (F) The histograms show the percentage of WT/R878H-derived HSCs in LIP group (red) and CTL group (black). n = 6–7 mice per group from two independent experiments. All data above are shown as mean ± SEM. *P < 0.05. All data were analyzed using a two-way ANOVA followed by Sidak's multiple comparisons test.

Figure 5 Activation of chemokine signaling in Dnmt3a R878H mutant myeloid cells in gingiva under periodontitis

(A–D) FACS sorting 3000 donor-derived myeloid cells ($CD45.2^+$ $CD11b^+$) from gingival tissues of recipient mice from Figure 2A. Then, these cells underwent RNA-seq for whole-genome transcriptome analysis. (A) The heatmap depicts representative genes specifically upregulated in R878H-LIP group shown in the Venn diagram as described in *Online Supplementary Figure S5C*. (B) Gene Ontology analysis upregulated genes for gingival myeloid cells of R878H recipients treated with LIP versus CTL. (C) Gene Ontology analysis upregulated genes for gingival myeloid cells of WT recipients treated with LIP versus CTL. (D) Gene set enrichment analysis (GSEA) of a curated list of chemokine activity target genes (*Online Supplementary Table S3*) in R878H and WT cells treated with LIP versus CTL. (E-F)

Quantitative real-time PCR (qPCR) was performed to confirm the expression of some chemokine-related genes (*Ccl4*, *Ccl22*, *Ccl17*) in the gingiva of recipient mice. All data above are shown as mean ± SEM and were analyzed using a two-way ANOVA followed by Sidak's multiple comparisons test.

Figure 6 Dnmt3a R878H drives systemic chemokine storm in periodontitis-associated clonal hematopoiesis

(A–D) The serum sample from the recipient mice in Figure 2A, and the serum in the same group pooled together to do cytokine array analysis. (A) The Venn diagram exhibits the upregulated proteins in R878H-LIP group when compared to R878H-CTL group, WT-LIP group and WT-CTL group, respectively. (B) Chemokines specifically upregulated in R878H-LIP group are shown in the heatmap. (C) Gene Ontology analysis for upregulated proteins in serum of R878H recipients treated with LIP versus CTL. (D) Gene Ontology analysis for upregulated proteins in serum of WT recipients treated with LIP versus CTL. (E-F) Enzyme-linked immunosorbent assays (ELISA) were performed to confirm the level of chemokines (CCL4, CCL17) in the serum of recipient mice (n = 4/group). (E) Experimental design. (F) The concentration of CCL4 and CCL17 in the serum of WT/R878H recipient mice with or without ligation. All data above are shown as mean ± SEM and were analyzed using a two-way ANOVA followed by Sidak's multiple comparisons test.

Figure 7 CCL17 expands R878H HSCs *in vitro*

(A–C) 400 HSCs ($CD48^-$ $CD150^+$ LSK) were freshly isolated from either WT or R878H mice, and the HSCs were cultured *in vitro* in the presence or absence of CCL4/CCL17 (100 ng/mL) for 6 days (all HSCs were cultured in SFEM medium supplemented with 30 ng/mL SCF, 30 ng/mL TPO and 100 U/mL Penicillin–Streptomycin). (A) Experimental design. (B–C) The cell number of live

cells (DAPI negative) and HSCs ($CD150^+$ $CD48^-$ c-KIT^+ $SCA\text{-}1^+$) was analyzed on days 6 (n = 4). (D) A model for the project. The Dnmt3a R878H mutation establishes a CCL17-associated feedback circuit linking periodontitis and clonal hematopoiesis by enhancing hematopoietic stem cells' capacity to exacerbate periodontal inflammation through myeloid hyperactivation and inflammatory stress resistance, thereby creating a self-amplifying pathogenic loop.

Figure 1

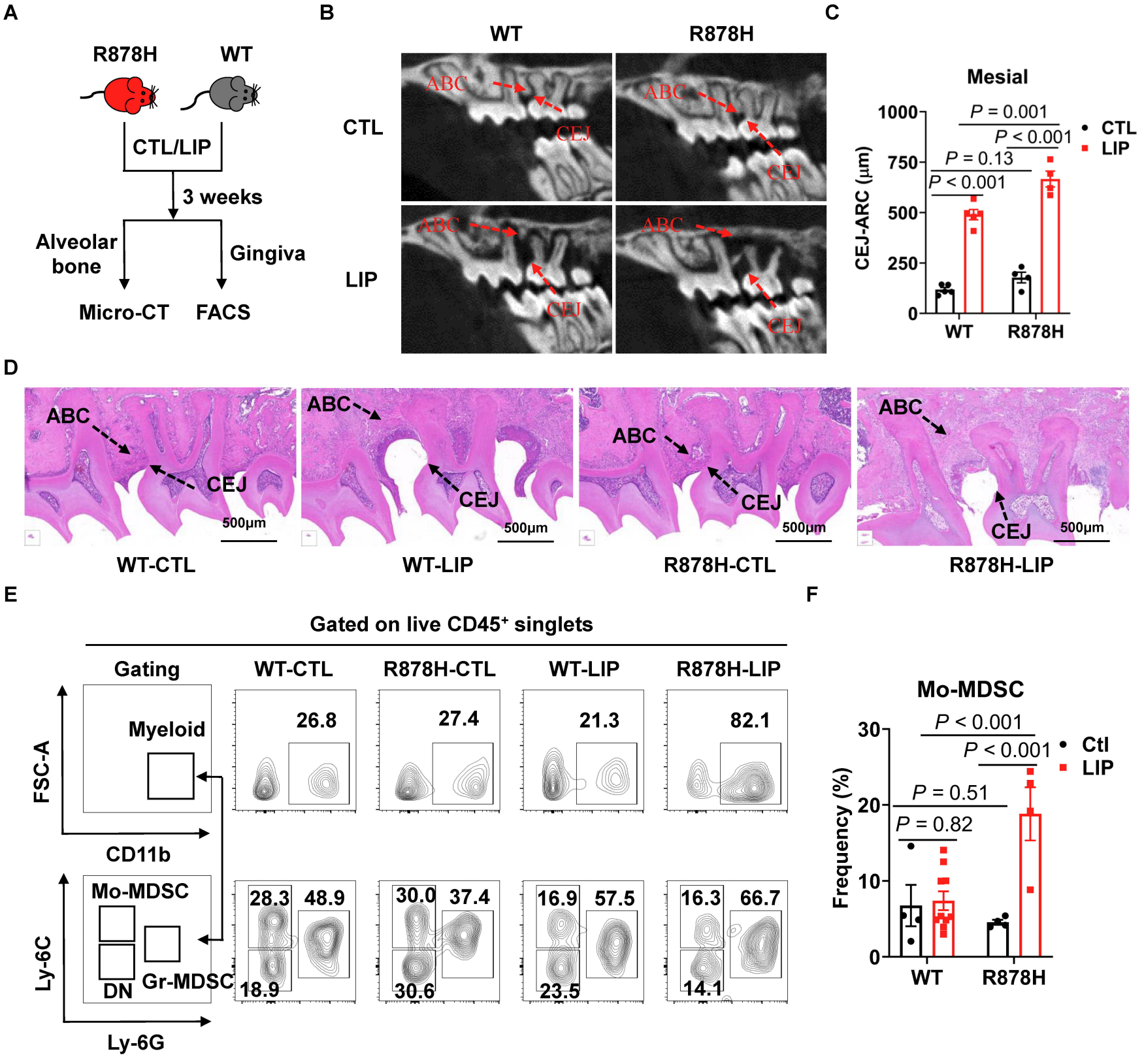
A
R878H
WT
CTL/LIP
3 weeks
Alveolar bone
Gingiva
Micro-CT
FACS
B
WT
R878H
CTL
LIP
ABC
CEJ
C
Mesial
CEJ-ARC (μm)
1000
750
500
250
0
P = 0.001
P < 0.001
P = 0.13
P < 0.001
CTL
LIP
WT
R878H
D
ABC
CEJ
500μm
WT-CTL
WT-LIP
R878H-CTL
R878H-LIP
E
Gated on live CD45+ singlets
Gating
WT-CTL
R878H-CTL
WT-LIP
R878H-LIP
Myeloid
FSC-A
CD11b
26.8
27.4
21.3
82.1
Mo-MDSC
Gr-MDSC
DN
Ly-6C
Ly-6G
28.3
48.9
18.9
30.0
37.4
30.6
16.9
57.5
23.5
16.3
66.7
14.1
F
Mo-MDSC
Frequency (%)
30
20
10
0
P < 0.001
P < 0.001
P = 0.51
P = 0.82
Ctl
LIP
WT
R878H

Figure 2

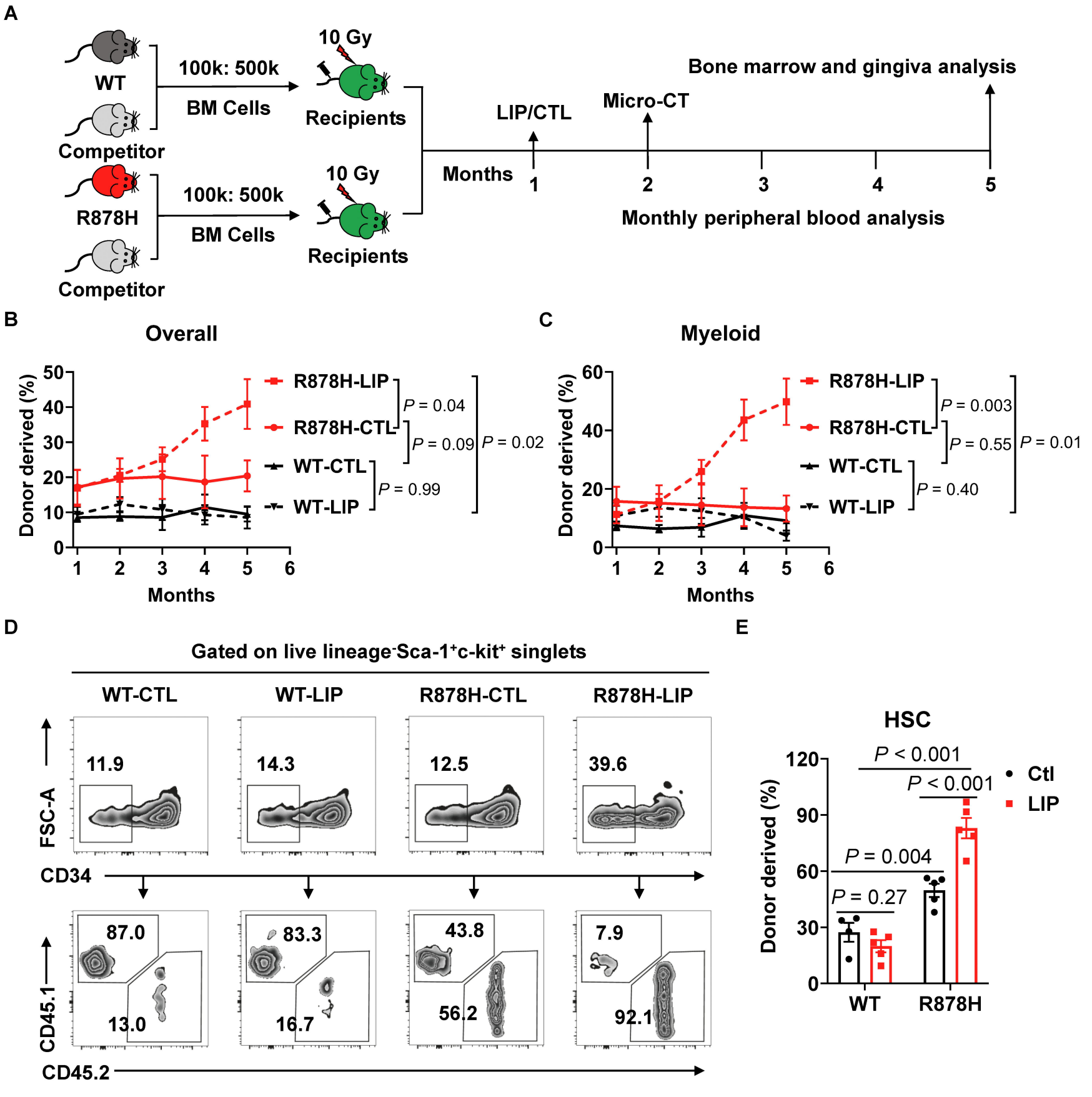
A
WT
Competitor
100k: 500k
BM Cells
10 Gy
Recipients
R878H
Competitor
100k: 500k
BM Cells
10 Gy
Recipients
LIP/CTL
Micro-CT
Bone marrow and gingiva analysis
Months
1
2
3
4
5
Monthly peripheral blood analysis
B
Overall
Donor derived (%)
R878H-LIP
R878H-CTL
WT-CTL
WT-LIP
P = 0.04
P = 0.09
P = 0.99
P = 0.02
Months
C
Myeloid
Donor derived (%)
R878H-LIP
R878H-CTL
WT-CTL
WT-LIP
P = 0.003
P = 0.55
P = 0.40
P = 0.01
Months
D
Gated on live lineage⁻Sca-1⁺c-kit⁺ singlets
WT-CTL
WT-LIP
R878H-CTL
R878H-LIP
FSC-A
11.9
14.3
12.5
39.6
CD34
CD45.1
87.0
13.0
83.3
16.7
43.8
56.2
7.9
92.1
CD45.2
E
HSC
Donor derived (%)
P < 0.001
P < 0.001
P = 0.004
P = 0.27
Ctl
LIP
WT
R878H

Figure 3

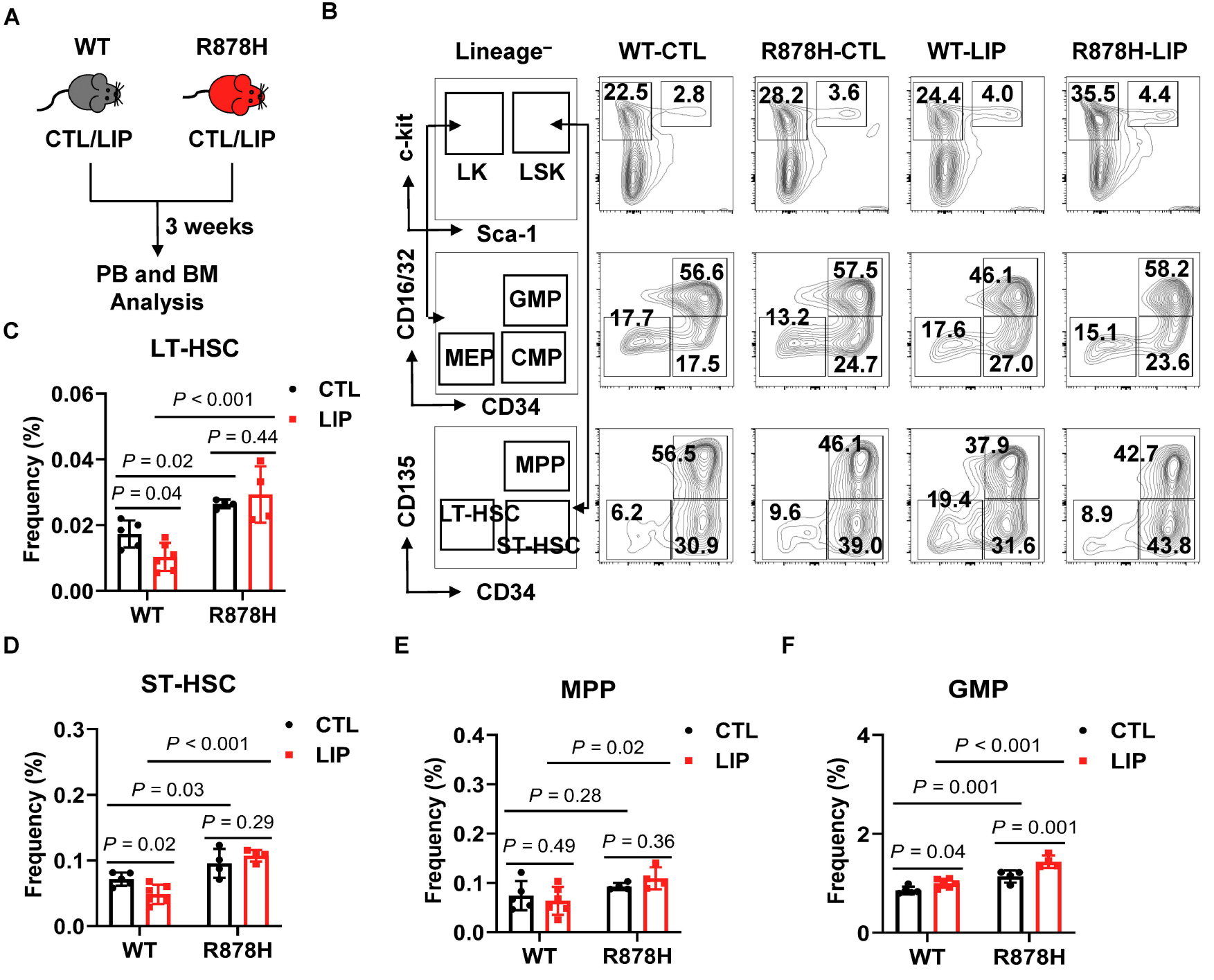
A
WT
R878H
CTL/LIP
CTL/LIP
3 weeks
PB and BM Analysis
B
Lineage⁻
WT-CTL
R878H-CTL
WT-LIP
R878H-LIP
c-kit
LK
LSK
Sca-1
CD16/32
GMP
MEP
CMP
CD34
CD135
MPP
LT-HSC
ST-HSC
CD34
22.5
2.8
28.2
3.6
24.4
4.0
35.5
4.4
56.6
17.7
17.5
57.5
13.2
24.7
46.1
17.6
27.0
58.2
15.1
23.6
56.5
6.2
30.9
46.1
9.6
39.0
37.9
19.4
31.6
42.7
8.9
43.8
C
LT-HSC
Frequency (%)
0.06
0.04
0.02
0.00
P < 0.001
P = 0.44
P = 0.02
P = 0.04
CTL
LIP
WT
R878H
D
ST-HSC
Frequency (%)
0.3
0.2
0.1
0.0
P < 0.001
P = 0.03
P = 0.29
P = 0.02
CTL
LIP
WT
R878H
E
MPP
Frequency (%)
0.4
0.3
0.2
0.1
0.0
P = 0.02
P = 0.28
P = 0.49
P = 0.36
CTL
LIP
WT
R878H
F
GMP
Frequency (%)
4
2
0
P < 0.001
P = 0.001
P = 0.001
P = 0.04
CTL
LIP
WT
R878H

Figure 4

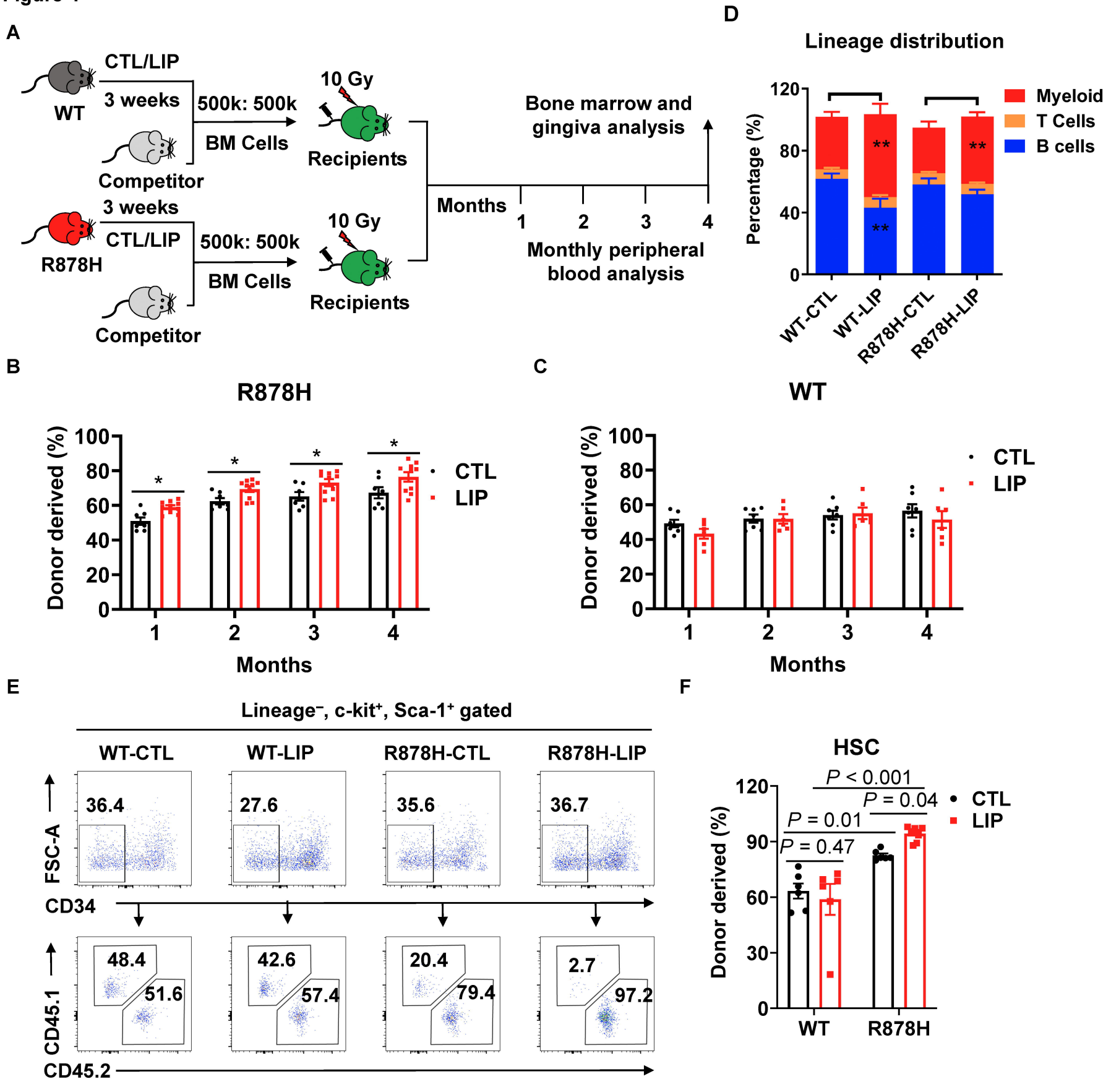
A
CTL/LIP
WT
3 weeks
500k: 500k
BM Cells
Competitor
10 Gy
Recipients
R878H
Bone marrow and gingiva analysis
Months
1
2
3
4
Monthly peripheral blood analysis
D
Lineage distribution
Percentage (%)
Myeloid
T Cells
B cells
WT-CTL
WT-LIP
R878H-CTL
R878H-LIP
B
R878H
Donor derived (%)
CTL
LIP
Months
C
WT
E
Lineage⁻, c-kit⁺, Sca-1⁺ gated
FSC-A
CD34
CD45.1
CD45.2
36.4
27.6
35.6
36.7
48.4
51.6
42.6
57.4
20.4
79.4
2.7
97.2
F
HSC
P < 0.001
P = 0.04
P = 0.01
P = 0.47

Figure 5

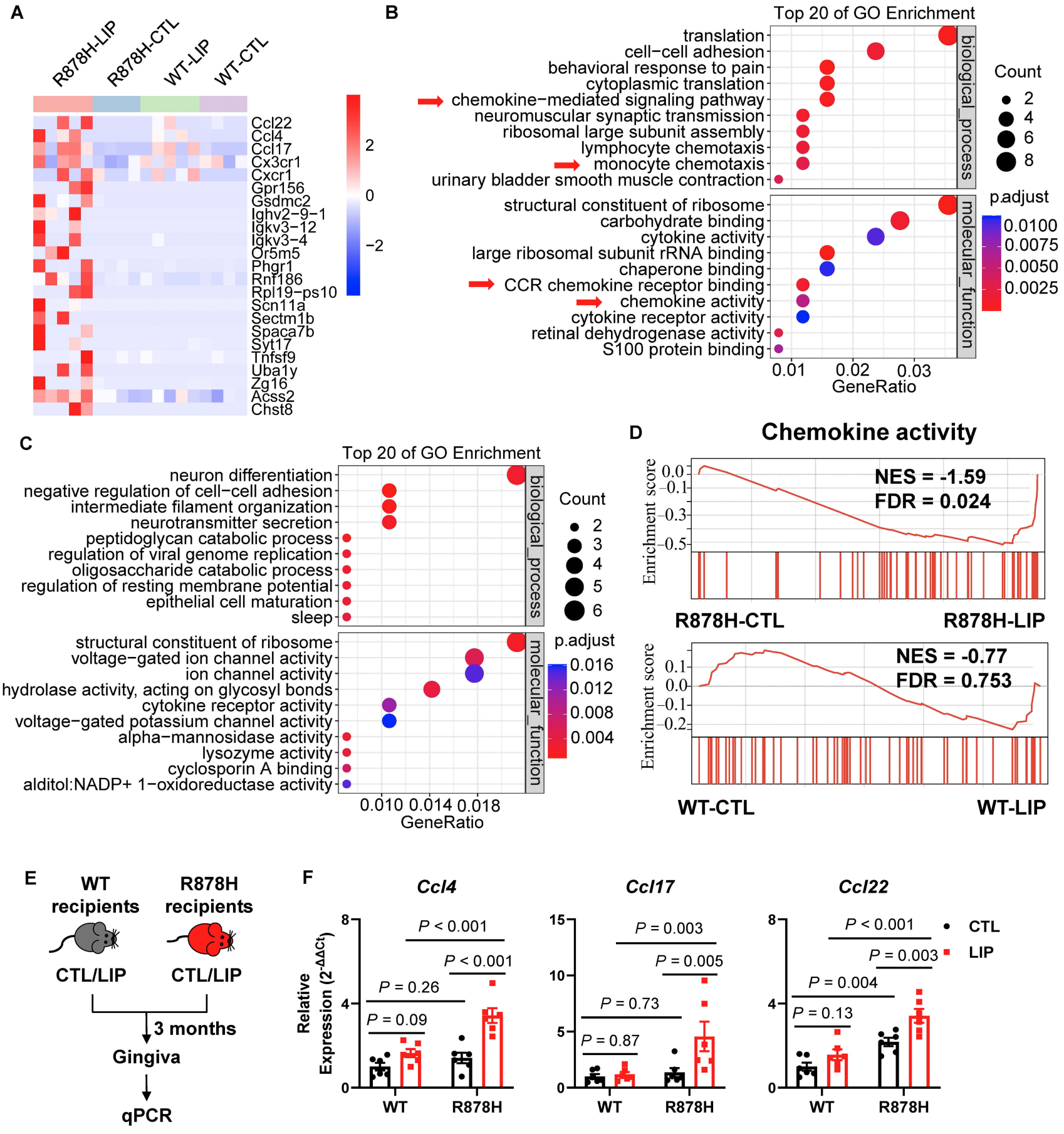
A
R878H-LIP
R878H-CTL
WT-LIP
WT-CTL
Ccl22
Ccl4
Ccl17
Cx3cr1
Cxcr1
Gpr156
Gsdmc2
Ighv2−9−1
Igkv3−12
Igkv3−4
Or5m5
Phgr1
Rnf186
Rpl19−ps10
Scn11a
Sectm1b
Spaca7b
Syt17
Tnfsf9
Uba1y
Zg16
Acss2
Chst8
2
0
−2
B
Top 20 of GO Enrichment
translation
cell−cell adhesion
behavioral response to pain
cytoplasmic translation
chemokine−mediated signaling pathway
neuromuscular synaptic transmission
ribosomal large subunit assembly
lymphocyte chemotaxis
monocyte chemotaxis
urinary bladder smooth muscle contraction
structural constituent of ribosome
carbohydrate binding
cytokine activity
large ribosomal subunit rRNA binding
chaperone binding
CCR chemokine receptor binding
chemokine activity
cytokine receptor activity
retinal dehydrogenase activity
S100 protein binding
biological_process
molecular_function
Count
2
4
6
8
p.adjust
0.0100
0.0075
0.0050
0.0025
0.01
0.02
0.03
GeneRatio
C
Top 20 of GO Enrichment
neuron differentiation
negative regulation of cell−cell adhesion
intermediate filament organization
neurotransmitter secretion
peptidoglycan catabolic process
regulation of viral genome replication
oligosaccharide catabolic process
regulation of resting membrane potential
epithelial cell maturation
sleep
structural constituent of ribosome
voltage−gated ion channel activity
ion channel activity
hydrolase activity, acting on glycosyl bonds
cytokine receptor activity
voltage−gated potassium channel activity
alpha−mannosidase activity
lysozyme activity
cyclosporin A binding
alditol:NADP+ 1−oxidoreductase activity
biological_process
molecular_function
Count
2
3
4
5
6
p.adjust
0.016
0.012
0.008
0.004
0.010 0.014 0.018
GeneRatio
D
Chemokine activity
Enrichment score
0.0
−0.1
−0.3
−0.5
NES = -1.59
FDR = 0.024
R878H-CTL
R878H-LIP
Enrichment score
0.1
0.0
−0.1
−0.2
NES = -0.77
FDR = 0.753
WT-CTL
WT-LIP
E
WT recipients
R878H recipients
CTL/LIP
CTL/LIP
3 months
Gingiva
qPCR
F
Ccl4
Ccl17
Ccl22
Relative Expression ($2^{-\Delta\Delta Ct}$)
P < 0.001
P < 0.001
P = 0.26
P = 0.09
P = 0.003
P = 0.005
P = 0.73
P = 0.87
P < 0.001
P = 0.003
P = 0.004
P = 0.13
CTL
LIP
WT
R878H
WT
R878H
WT
R878H

Figure 6

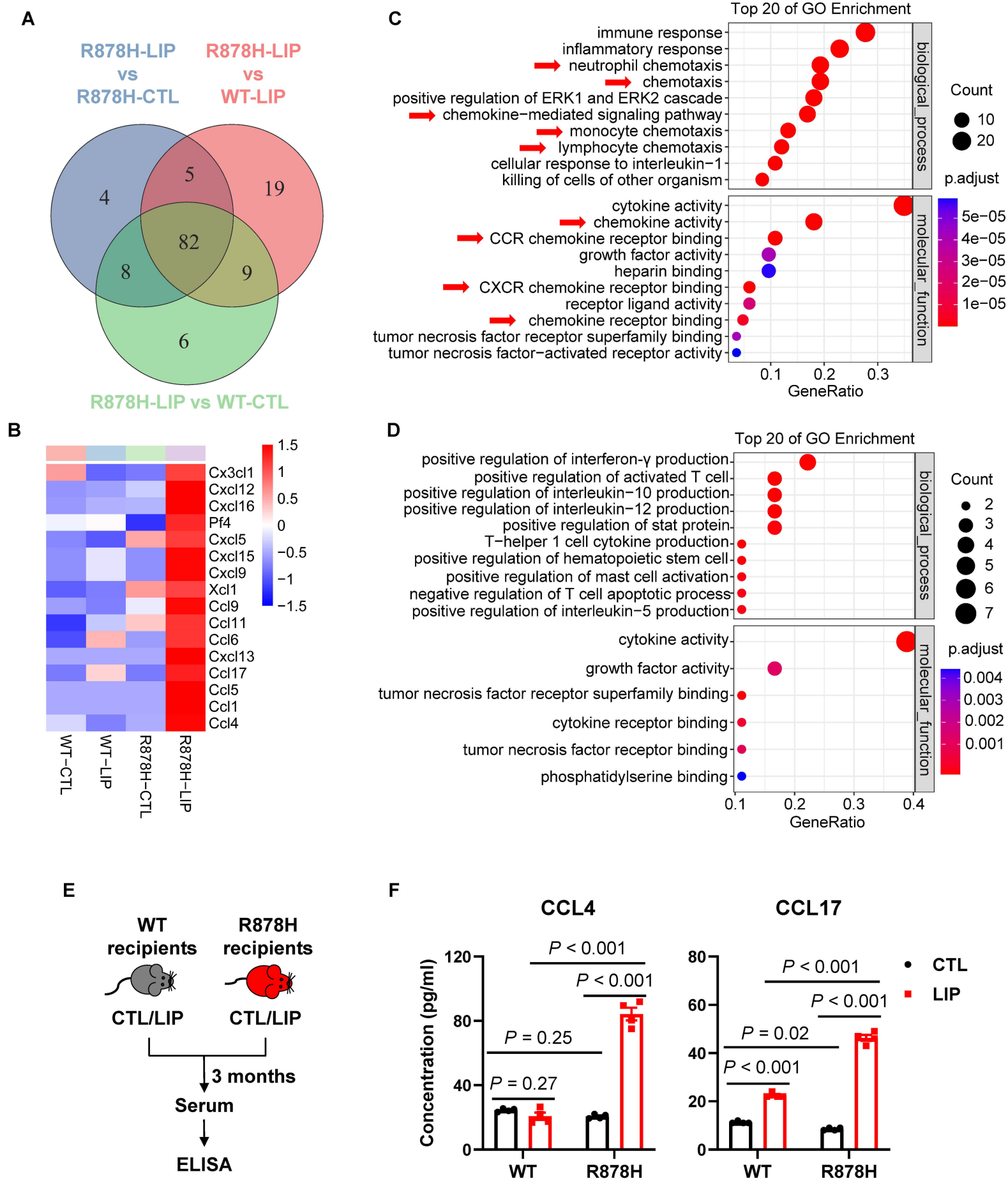
A
R878H-LIP vs R878H-CTL
R878H-LIP vs WT-LIP
R878H-LIP vs WT-CTL
4
5
19
82
8
9
6
B
Cx3cl1
Cxcl12
Cxcl16
Pf4
Cxcl5
Cxcl15
Cxcl9
Xcl1
Ccl9
Ccl11
Ccl6
Cxcl13
Ccl17
Ccl5
Ccl1
Ccl4
1.5
1
0.5
0
−0.5
−1
−1.5
WT−CTL
WT−LIP
R878H−CTL
R878H−LIP
C
Top 20 of GO Enrichment
immune response
inflammatory response
neutrophil chemotaxis
chemotaxis
positive regulation of ERK1 and ERK2 cascade
chemokine−mediated signaling pathway
monocyte chemotaxis
lymphocyte chemotaxis
cellular response to interleukin−1
killing of cells of other organism
biological_process
cytokine activity
chemokine activity
CCR chemokine receptor binding
growth factor activity
heparin binding
CXCR chemokine receptor binding
receptor ligand activity
chemokine receptor binding
tumor necrosis factor receptor superfamily binding
tumor necrosis factor−activated receptor activity
molecular_function
0.1
0.2
0.3
GeneRatio
Count
10
20
p.adjust
5e−05
4e−05
3e−05
2e−05
1e−05
D
Top 20 of GO Enrichment
positive regulation of interferon-γ production
positive regulation of activated T cell
positive regulation of interleukin−10 production
positive regulation of interleukin−12 production
positive regulation of stat protein
T−helper 1 cell cytokine production
positive regulation of hematopoietic stem cell
positive regulation of mast cell activation
negative regulation of T cell apoptotic process
positive regulation of interleukin−5 production
biological_process
cytokine activity
growth factor activity
tumor necrosis factor receptor superfamily binding
cytokine receptor binding
tumor necrosis factor receptor binding
phosphatidylserine binding
molecular_function
0.1
0.2
0.3
0.4
GeneRatio
Count
2
3
4
5
6
7
p.adjust
0.004
0.003
0.002
0.001
E
WT recipients
R878H recipients
CTL/LIP
CTL/LIP
3 months
Serum
ELISA
F
CCL4
CCL17
Concentration (pg/ml)
120
80
40
0
P < 0.001
P < 0.001
P = 0.25
P = 0.27
80
60
40
20
0
P < 0.001
P < 0.001
P = 0.02
P < 0.001
WT
R878H
CTL
LIP

Figure 7

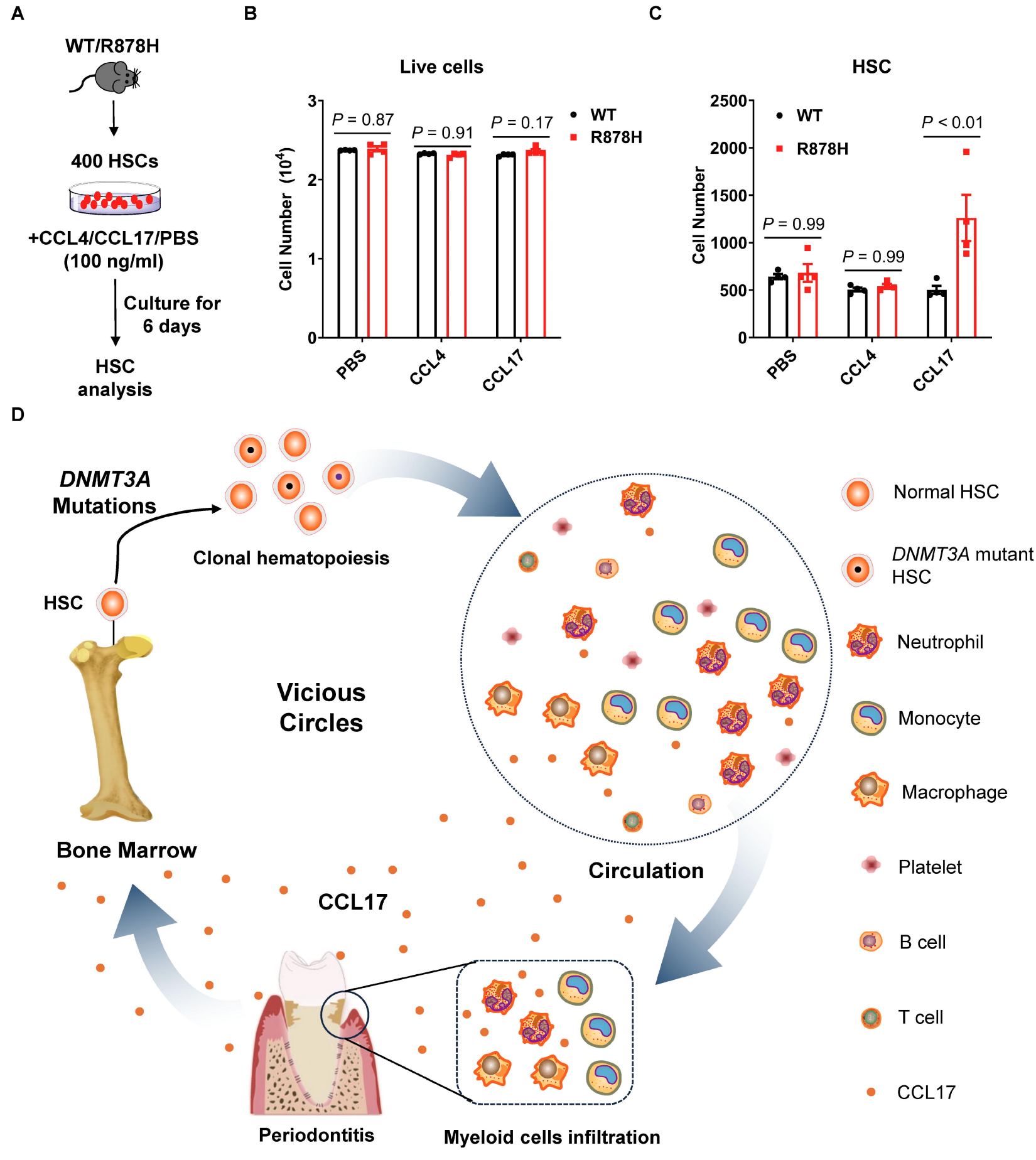
A
WT/R878H
400 HSCs
+CCL4/CCL17/PBS
(100 ng/ml)
Culture for
6 days
HSC
analysis
B
Live cells
Cell Number (10^4)
P = 0.87
P = 0.91
P = 0.17
WT
R878H
PBS
CCL4
CCL17
C
HSC
Cell Number
P = 0.99
P = 0.99
P < 0.01
WT
R878H
PBS
CCL4
CCL17
D
DNMT3A
Mutations
Clonal hematopoiesis
HSC
Bone Marrow
Vicious
Circles
Circulation
CCL17
Periodontitis
Myeloid cells infiltration
Normal HSC
DNMT3A mutant
HSC
Neutrophil
Monocyte
Macrophage
Platelet
B cell
T cell
CCL17

Methods

In Vivo Micro-Computed Tomography (Micro-CT)

Mice were anesthetized by inhalation of 2% isoflurane delivered in air and positioned for scanning. The maxillae were subsequently imaged using an *in vivo* micro-computed tomography (micro-CT) system (SkyScan 1172, Bruker). Scans were acquired at an isotropic voxel resolution of 18 μm. Projection images were reconstructed into cross-sectional slices using the manufacturer's software (DataViewer v1.5.6.2, Bruker). To quantify alveolar bone loss, the distance from the cementoenamel junction (CEJ) to the alveolar bone crest (ABC) was measured on mesial, buccal, distal and palatal surfaces of the maxillary second molars within the reconstructed images using DataViewer software (version 1.5.4.0, Bruker, Germany).

Histological analysis of periodontal tissue

After being decalcified in 10% EDTA solution (pH 7.2) for 4 weeks, the maxillae were sectioned and stained with hematoxylin and eosin (H&E) or tartrate-resistant acid phosphatase (TRAP). The stained sections were scanned using a Pannoramic MIDI II scanner (3DHISTECH).

Cells preparations and sample collection

During preparation of BM single-cell suspensions, mouse femurs were flushed with chilled $HBSS^+$ buffer (Hank's balanced salt solution supplemented with 2% fetal bovine serum, 1% penicillin/streptomycin, and 1% HEPES). Cells were forced through a 70-μm nylon cell strainer to obtain single-cell suspensions for subsequent flow cytometric analysis and fluorescence-activated cell sorting (FACS). To collect BM extracellular fluid, femurs were rinsed with 500 μL ice-cold PBS (Gibco, Thermo Fisher Scientific), followed by centrifugation at 500× g for 5 minutes at 4°C to harvest supernatants.

Peripheral blood (PB) mature cells were lysed with ACK buffer (NH_4Cl 150 mM, $KHCO_3$ 10 mM, Na_2EDTA 0.1 mM, adjust the pH to 7.2–7.4), followed by staining for chimerism analysis using flow cytometry. Serum was collected via retro-orbital bleeding. Specifically, whole blood was allowed to clot undisturbed at room temperature for 30 minutes, centrifuged at 12000× g for 10 minutes at 4°C to remove clots, and the supernatant was subsequently harvested.

Gingival tissues around the area of ligature placement (and the contralateral control area) were dissected within 3 minutes post-euthanasia and digested with cold PBS (Gibco, Thermo Fisher Scientific) supplemented with 2% FBS (Gibco). Gingival tissues were then cut into 1-mm^2 pieces with scissor and digested in freshly prepared digestion medium consisting of 2 mg/ml collagenase type II (Yeasen) and 1 mg/ml DNase I (Yeasen). The digestion was performed at 37°C with orbital shaking at 200 rpm for 30 minutes and subsequently quenched by adding EDTA (Invitrogen, Thermo Fisher Scientific) to a final concentration of 5 mM. Single-cell suspensions were obtained by mechanically disrupting the tissues through a 70-μm nylon mesh using a syringe plunger, followed by filtration for subsequent staining for FACS analysis.

Flow cytometry and sorting

Flow cytometry analysis was performed on a Sony SA3800 flow cytometer (Sony) and analyzed using FlowJo™ software (Becton, Dickinson and Company). Cell sorting was conducted with the Sony SH800s internal sorter, with target populations sorted into $HBSS^+$ buffer. Non-lysed BM cells were used for hematopoietic stem and progenitor cell (HSPC) analysis (antibodies included lineage-biotin cocktail, streptavidin APC-Cy™7, c-kit APC, Sca-1 PE/Cy7, CD150 PE, CD34 Alexa Fluor 700, CD16/32 FITC, and CD135 PE-CF594) and lineage analysis (antibodies targeting CD11b, Gr1, B220, and CD3). PB mature cell chimerism analysis included antibodies against CD11b, B220, CD3, CD45.1 and CD45.2. A detailed list of antibodies is provided in *Online Supplementary Information Table S1*.

Bone marrow transplantation

BM cells were isolated from *Dnmt3a*$^{R878H/+}$*Vav1*-cre$^+$ mice (R878H, CD45.2) and *Dnmt3a*$^{R878H/+}$*Vav1*-cre$^-$ littermates (WT, CD45.2), as well as congenic WT (CD45.1) mice. As shown in Figure 2A, in the experimental group, lethally irradiated (10 Gy) CD45.1/2 recipient mice received 1×10^5 R878H or WT BM cells mixed with 5×10^5 WT CD45.1 BM cells. 1 month after BM transplantation, 50% of R878H and WT recipient mice received LIP. Peripheral blood from recipients was analyzed monthly for donor-derived chimerism (myeloid cells, B cells and T cells). An antibody panel (CD3, B220, CD11b, CD45.1 and CD45.2) was used to assess peripheral blood chimerism.

UID mRNA-seq and data analysis

Gingival $CD45.2^+$ and $CD11b^+$ cells were isolated using the Sony SH800s internal cell sorter from R878H recipients and WT recipients. All procedures involving unique molecular identifier (UID) mRNA analysis, including library preparation and high-throughput sequencing of the sorted cells, were performed by Wuhan Kangce Technology Co., Ltd. Total RNA was extracted from the sorted cells using TRIzol® Reagent (Thermo Fisher, cat. no. 15596026) following the manufacturer's protocol. To eliminate genomic DNA contamination, extracted RNA samples were treated with DNase I (NEB, cat. no. M0303L). RNA purity was assessed by measuring A260/A280 ratios on a NanoDrop™ OneC spectrophotometer (Thermo Fisher), while RNA integrity was verified using the LabChip® GX Touch system (Revvity). Subsequently, RNA concentration was accurately quantified using a Qubit® 3.0 Fluorometer with the Qubit™ RNA Broad Range Assay Kit (Thermo Fisher, cat. no. Q10210). For RNA sequencing library construction, total RNA was processed with the KC™ Digital mRNA Library Prep Kit (Seqhealth Tech. Co., Ltd, Wuhan, China) according to the manufacturer's specifications. Final enriched libraries were quantified and subjected to paired-end 150-bp (PE150) sequencing on the DNBSEQ-T7 platform (MGI).

Cytokine antibody array

Serum samples were collected from recipient mice via retro-orbital venous plexus bleeding. Whole blood was clotted at room temperature for 30 min without disturbance, followed by centrifugation at 12,000 × g for 15 min at 4°C to remove coagulated material. The supernatant (serum) was collected, aliquoted into single-use vials, and stored at -80°C until analysis. Prior to detection, samples were subjected to 2-fold dilution and analyzed using a mouse antibody array kit (QAM-CAA-4000, RayBiotech). This glass chip-based platform simultaneously quantifies 200 cytokine proteins through immobilized antibody capture.

Quantitative real-time PCR

Total RNA was extracted from gingival cells using TRIzol® reagent (Invitrogen) following the manufacturer’s instructions. RNA concentrations were normalized, and cDNA was synthesized using the PrimeScript™ RT Reagent Kit (Takara, Cat #

RR047A). The resulting cDNA was analyzed on a QuantStudio™ 3 Real-Time PCR System (Applied Biosystems) with PowerUp™ SYBR™ Green Master Mix (Applied Biosystems, Cat # A25780) and specified primers. For full primer sequences, refer to *Online Supplementary Table S2*.

Statistical analysis

After confirming normality, data were analyzed using a two-way ANOVA followed by Sidak's multiple comparisons test. All statistical analyses were performed with GraphPad Prism software (version 8; GraphPad Inc.). All data are shown as mean ± SEM. *P*-value <0.05 was considered statistically significant.

Supplemental Figures and Figure legends

Fig. S1

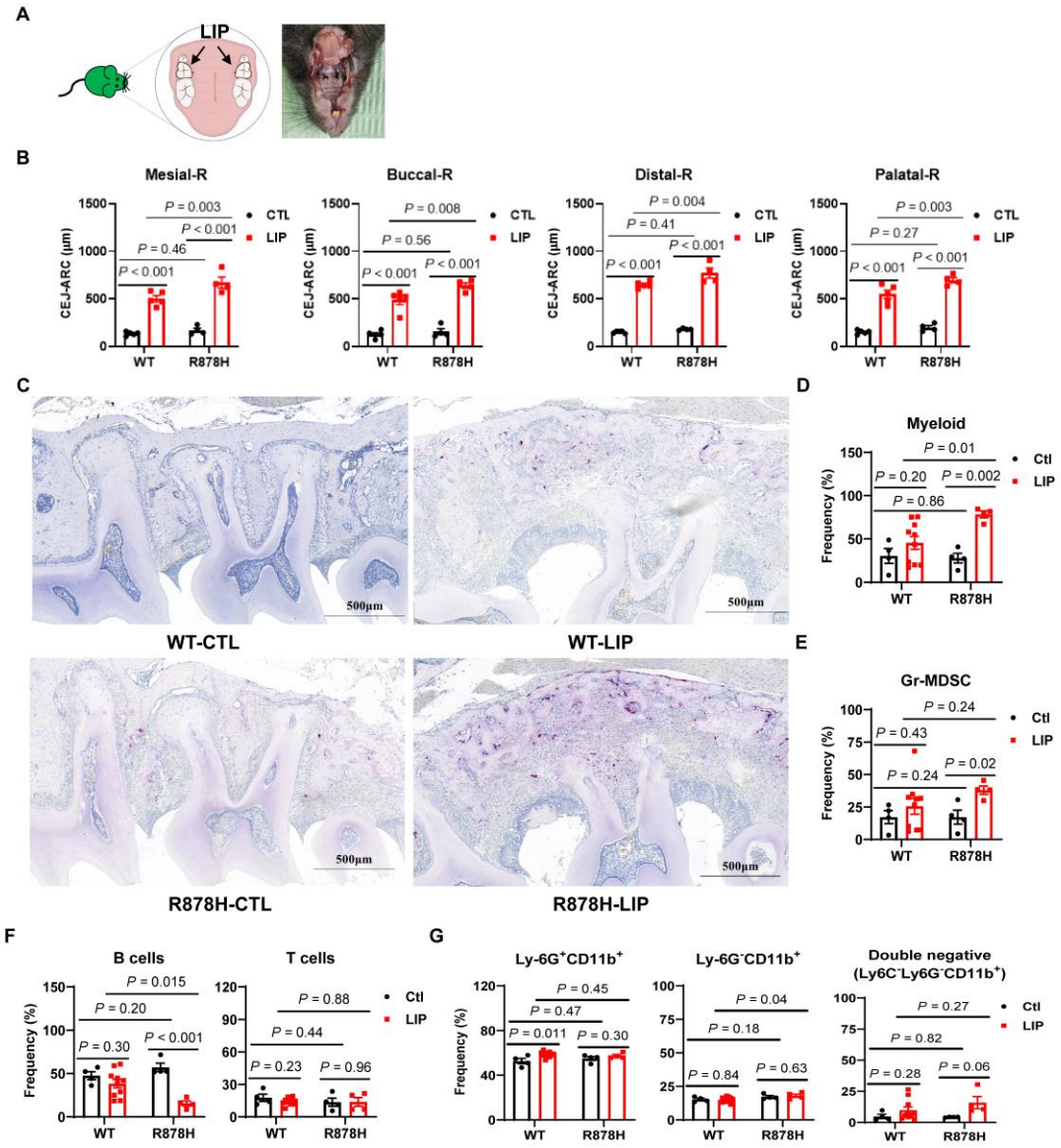

Figure S1 Dnmt3a R878H accelerates alveolar bone resorption and infiltration of gingival inflammatory cells

(A) Schematic diagram and image of LIP. (B) Site-specific CEJ-ABC measurements (mesial, buccal, distal, palatal) of maxillary right second molars across groups. (C) Quantification of osteoclasts by tartrate-resistant acid phosphatase (TRAP) staining around the maxillary second molar. (D-F) The frequency of cell population in gingival tissues: (D) myeloid cells ($CD45^+$ $CD11b^+$), (E) Gr-MDSC, (F) B cells and T cells, (G)The frequency of $CD45^+$ $Ly6G^+$ $CD11b^+$ cells, $CD45^+$ $Ly6G^-$ $CD11b^+$ cells and $CD45^+$ $Ly6C^-$ $Ly6G^-$ $CD11b^+$ cells in gingival tissues. n = 4–5 mice (2–3 months) per

group from two independent experiments. All data above are shown as mean ± SEM and were analyzed using a two-way ANOVA followed by Sidak's multiple comparisons test.

Fig. S2

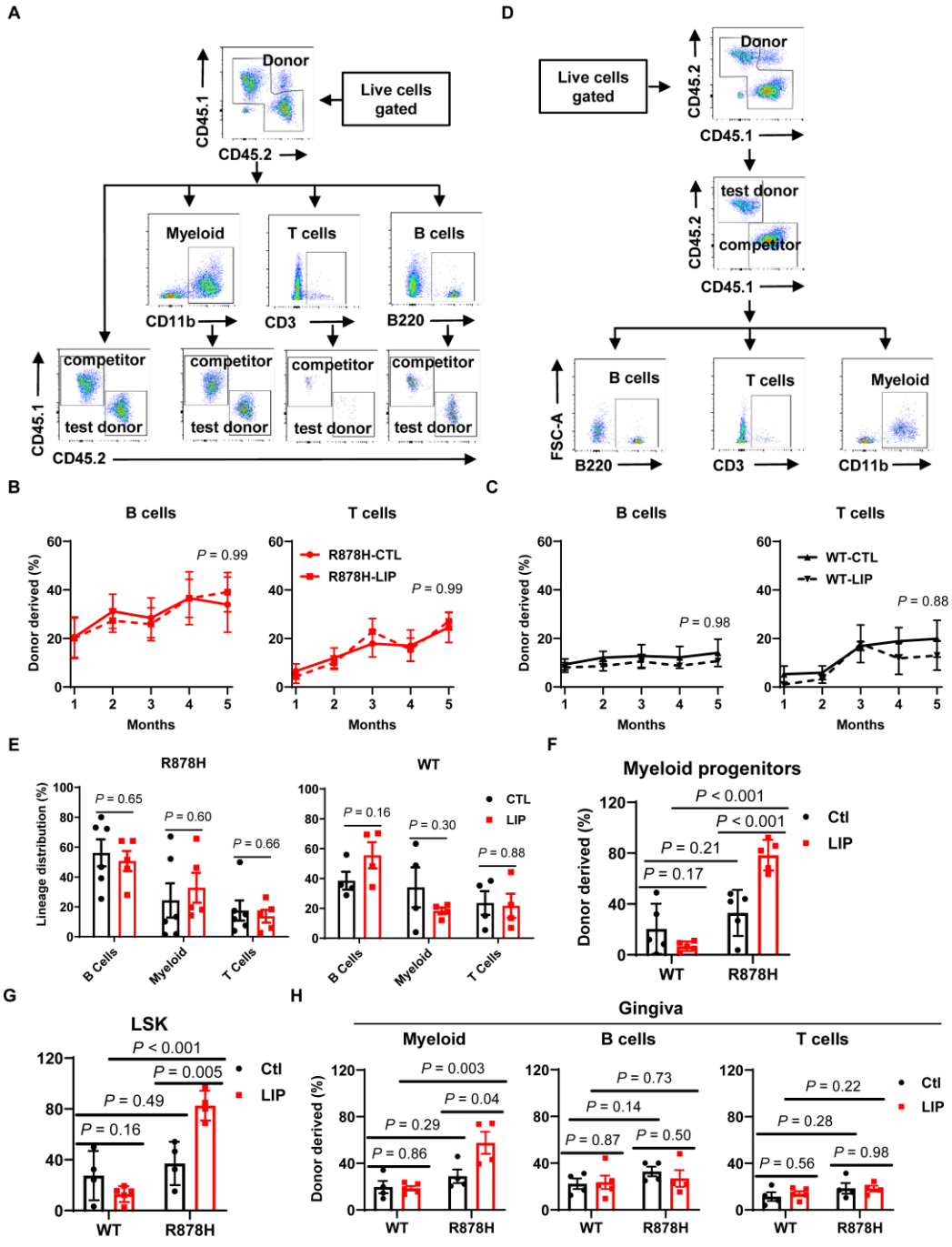

Figure S2 Ligature-induced periodontitis promotes Dnmt3a R878H-driven clonal hematopoiesis via a myeloid-biased phenotype

(A) Representative FACS plots identifying donor-derived ($CD45.2^+$) contribution to myeloid cells ($CD11b^+$), T cells ($CD3^+$) cells and B cells ($B220^+$) from R878H and WT mice. (B–C) Donor-derived ($CD45.2^+$) contribution to B cells ($B220^+$) and T cells ($CD3^+$) from R878H (B) and WT (C) mice. (D) Representative FACS plots identifying lineage distribution to B cells ($B220^+$), T cells ($CD3^+$) cells and myeloid cells ($CD11b^+$) in the bone marrow of recipients at the fifth month after transplantation. (E) Lineage distribution of B cells, myeloid cells and T cells among donor-derived cells in the PB of recipients carrying R878H or WT BM cells treated with or without LIP at the 5^{th} month after transplantation. (F–G) The histograms show the percentage of myeloid progenitor cells (F) and LSK (G) in LIP group (red) and CTL group (black) in the bone marrow. (H) The percentage of R878H/WT-derived myeloid cells ($CD11b^+$), B cells ($B220^+$) and T cells ($CD3^+$) within gingival tissue of indicated recipient mice. All data above are shown as mean ± SEM and were analyzed using a two-way ANOVA followed by Sidak's multiple comparisons test.

Fig. S3

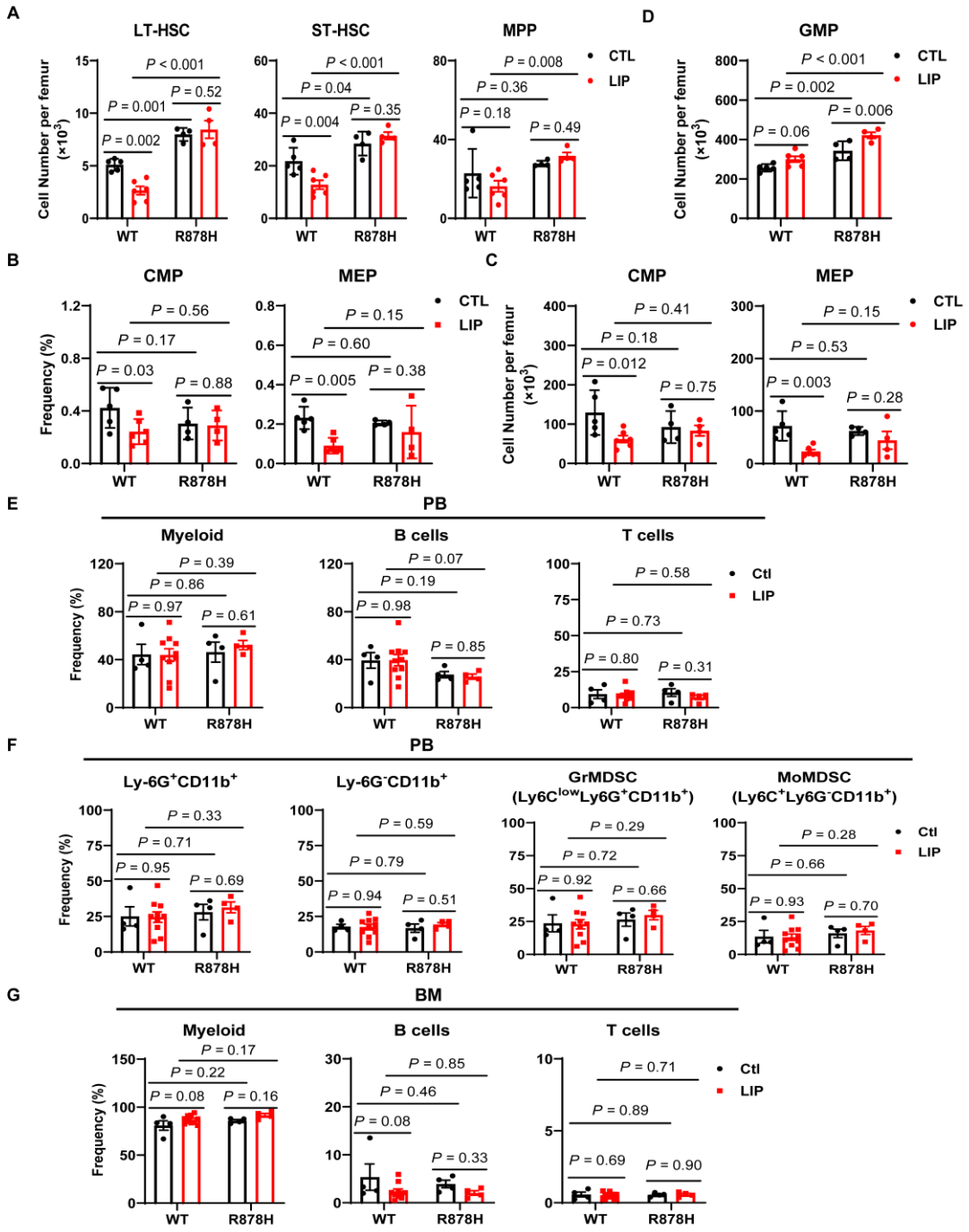

Figure S3 R878H HSCs exhibit greater resistance to inflammation induced by periodontitis than WT HSCs

(A) Histogram of absolute counts for BM populations: LT-HSCs, ST-HSCs and MPPs. (B–C) Histograms showing the frequency (B) and absolute count (C) of CMPs and MEPs in the bone marrow. (D) Histogram showing absolute counts of GMPs in bone

marrow. (E) The frequency of lineage cells (myeloid, B and T cells) in peripheral blood. (F) The frequency of Ly-6G$^+$ CD11b$^+$cells, Ly-6G$^-$ CD11b$^+$cells, Gr-MDSC (Ly6C^{low} Ly6G$^+$ CD11b$^+$) and Mo-MDSC (Ly6C$^+$ Ly6G$^-$ CD11b$^+$) in the peripheral blood of WT and R878H mice treated with or without LIP. (G) Frequency of myeloid cells (CD11b$^+$), B cells (B220$^+$) and T cells (CD3$^+$) of WT and R878H mice subjected or not (control) to LIP for 21 days in the BM. n = 4–5 mice per group from two independent experiments. All data above are shown as mean ± SEM and were analyzed using a two-way ANOVA followed by Sidak's multiple comparisons test.

Fig. S4

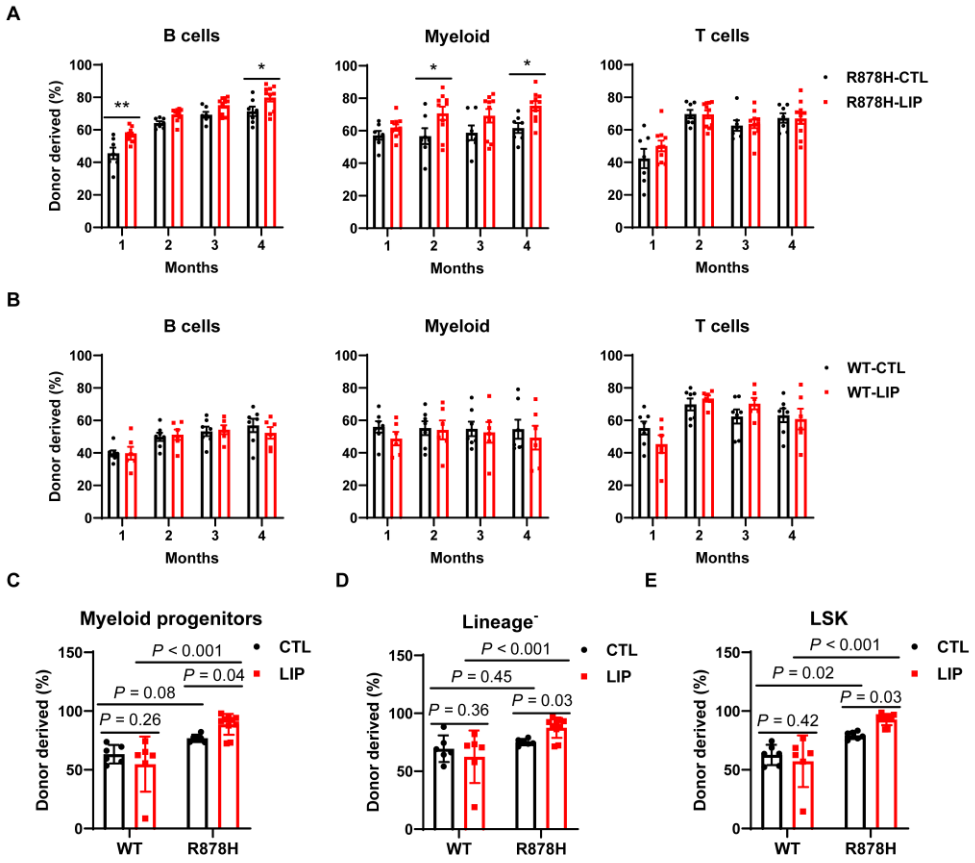

Figure S4 LIP-stressed R878H HSCs maintain a competitive advantage and a myeloid-biases differentiation

(A–B) Donor-derived (CD45.2$^+$) contribution to B cells (B220$^+$), myeloid cells (CD11b$^+$) and T cells (CD3$^+$) from R878H (A) and WT (B) recipient mice subjected, or not (control), to LIP. (C–E) The histograms show the percentage of WT/R878H-

derived myeloid progenitor cells (lineage$^-$ Sca-1$^-$ c-kit$^+$) (C) lineage$^-$ (D) and LSK (E) in LIP group (red) and CTL group (black). n = 6–7 mice per group from two independent experiments. All data above are shown as mean ± SEM. *P < 0.05, **P < 0.01. All data were analyzed using a two-way ANOVA followed by Sidak's multiple comparisons test.

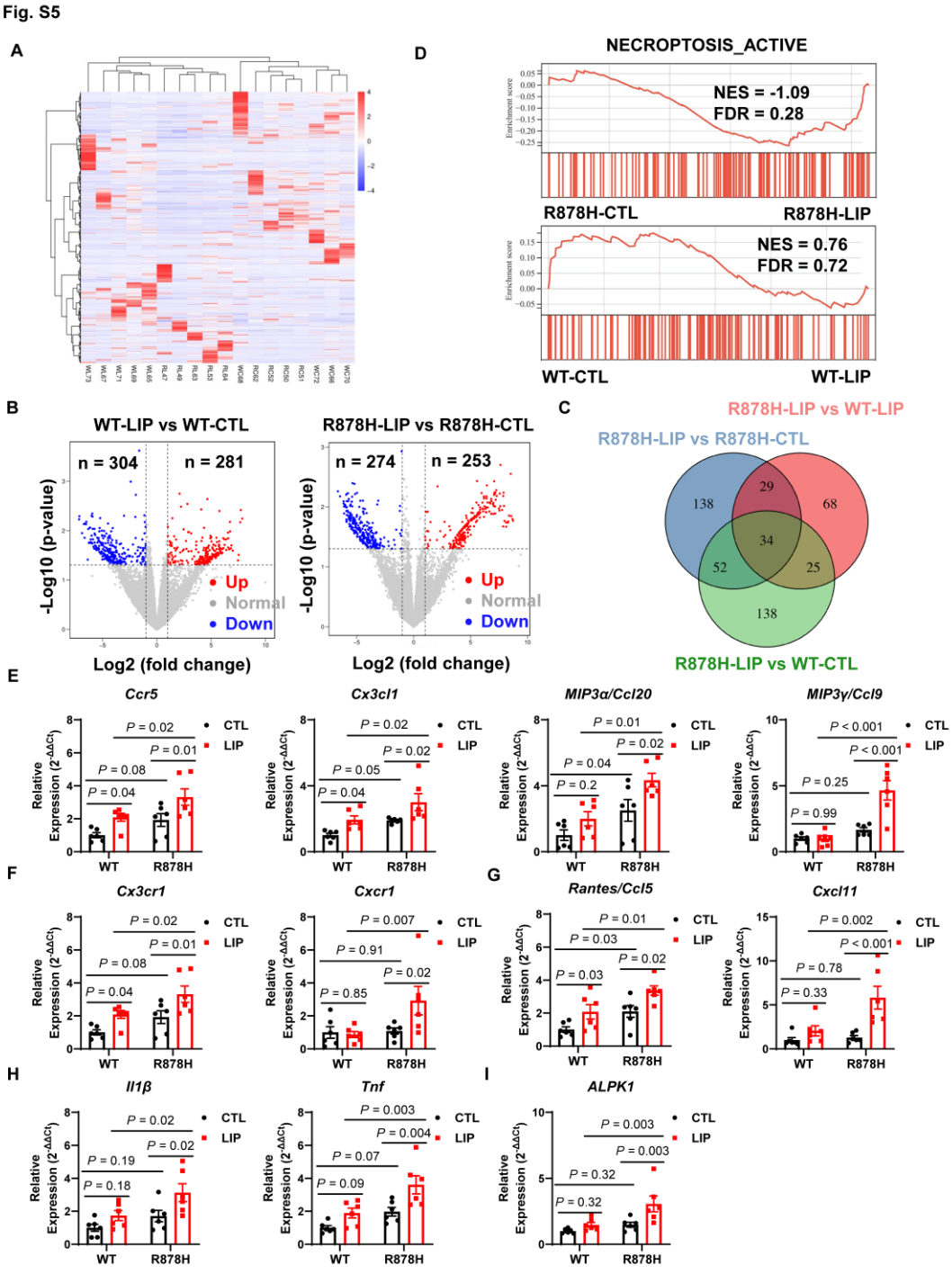

Figure S5 Activation of chemokine signaling in Dnmt3a R878H mutant myeloid

cells in gingiva under periodontitis

(A) The heatmap of differential expressed genes in each group. (B) All differentially expressed genes are shown in volcano plot. Highlighted genes in color (blue: downregulated, red: upregulated) are more than twofold differentially expressed ($P < 0.05$) in WT-LIP versus WT-CTL and R878H-LIP versus R878H-CTL groups. $n = 3$ independent mice per group. (C) The Venn diagram shows the upregulated genes in R878H-LIP group when compared to R878H-CTL group, WT-LIP group and WT-CTL group, respectively. (D) Gene set enrichment analysis (GSEA) of necroptosis activation-related genes in R878H and WT cells treated with LIP versus CTL. (E-I) Quantitative real-time PCR (qPCR) was performed to confirm the expression of some chemokine-related genes (*Ccr5*, *Cx3cl1*, *Ccl20*, *Ccl9*, *Cx3cr1*, *Cxcr1*, *Ccl5, Cxcl11*, *Il1β*, *Tnf* and *Alpk1*) in the gingiva of recipient mice. All data above are shown as mean ± SEM and were analyzed using a two-way ANOVA followed by Sidak's multiple comparisons test.

Fig. S6

A

Chemokines	Cxcl15, Cxcl9, Cxcl16, Ccl4, Ccl6, Cx3cl1, Cxcl5, Pf4, Ccl11, Cxcl12, Xcl1, Cxcl13, Ccl17, Ccl5, Ccl1, Ccl9, Cxcl11
Interleukins	Il17f, Il33, Il17b, Il1rn, Il22, Il2ra, Il1rl1, Il7, Cd40l, Csf2rb2
TNF superfamily	Tnfsf11, Tnfrsf19, Tnfrsf12a, Tnfrsf11b, Tnfsf18, Tnfrsf13c, Tnfrsf1a, Tnfrsf1b, Fas
Growth factors	SCF, Vegfa, Egf, Flt1, Hgf, Acvrl1, Areg, Igfbp5, Igfbp2
Adhesion molecules	Icam1, F11r, Madcam1
Others	Ctla4, Trem1, Gpnmb, Cdh3, Mme, Cd36, Prl, Clu, Chrd, Lgals1, Igdcc4, Cst3, Prss8, Gas1, Ren1, Dcn, Cd48, Dkk1, Spint1, Cd6, Gas6, Ace, Cd80, Kremen1, Ctf1, Ereg, Postn, Metrn, Mbl2, Dll4, Ahsg, Spp1, Adamts1, Gzmb

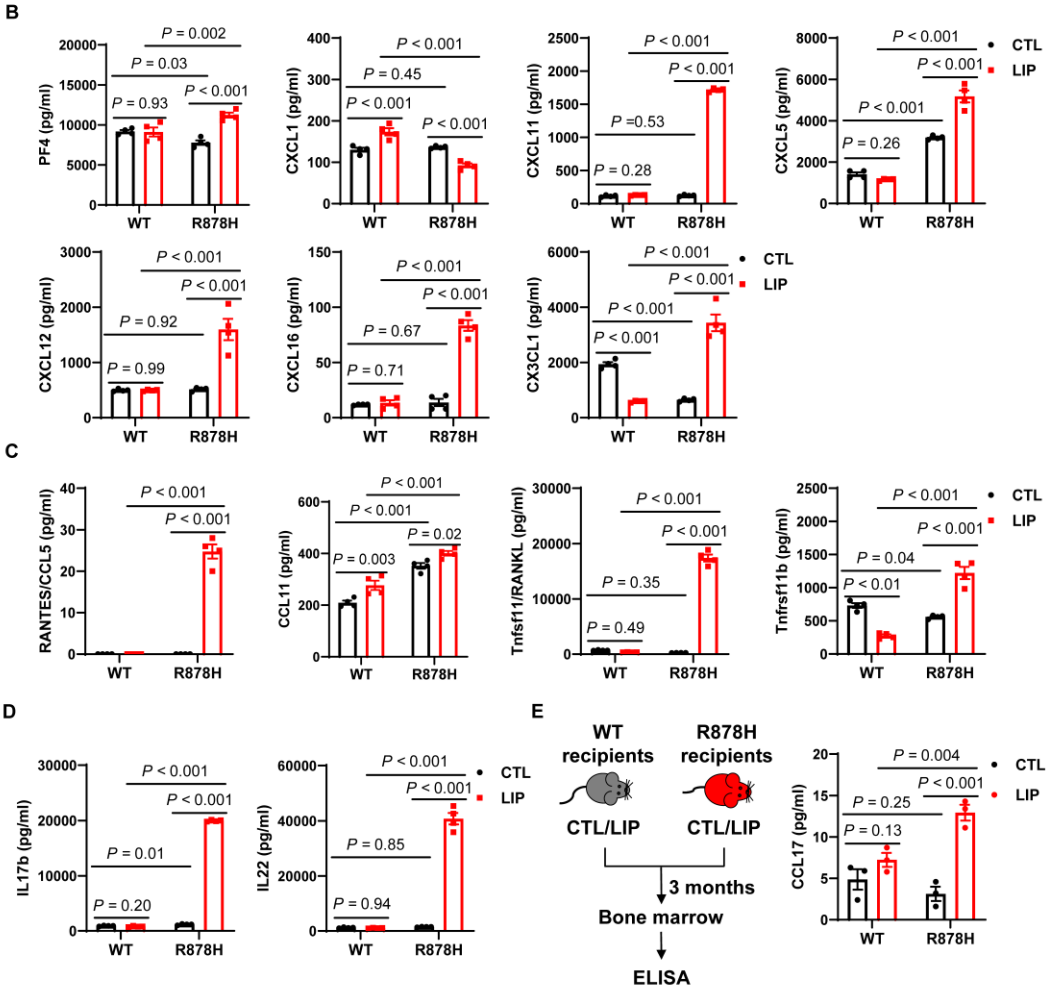

Figure S6 Dnmt3a R878H drives systemic chemokine storm in periodontitis associated clonal hematopoiesis

(A) The table depicts the proteins specifically upregulated in R878H-LIP group shown in the Venn diagram. (B–D) ELISA results show the level of chemokines (PF4, CXCL1, CXCL11, CXCL5, CXCL12, CXCL16, CX3CL1, CCL5, CCL11) and cytokines (RANKL, TNFRSF11b, IL17b, IL22) in the serum of recipient mice (n = 4/group). (E) ELISA was performed to confirm the level of CCL17 in the bone marrow of recipient

mice (n = 3/group). All data above are shown as mean ± SEM and were analyzed using a two-way ANOVA followed by Sidak's multiple comparisons test.

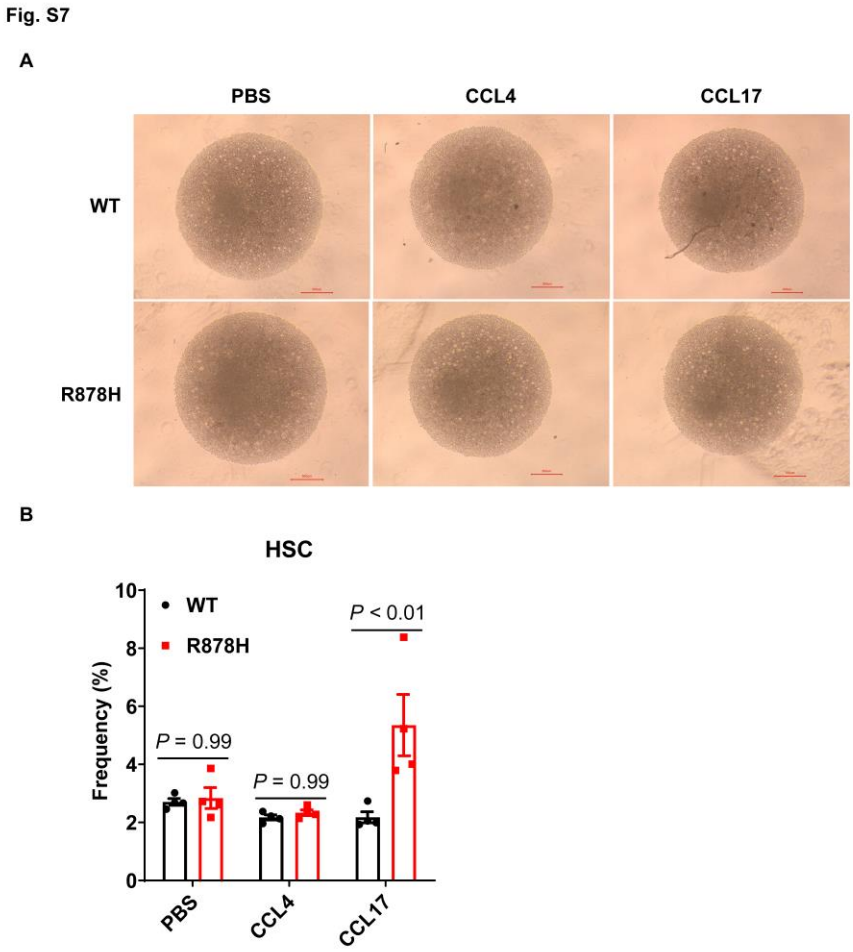

Figure S7 CCL17 expands R878H HSCs *in vitro*

(A–B) 400 HSCs ($CD48^{-}$ $CD150^{+}$ LSK) were freshly isolated from either WT or R878H mice, and the HSCs were cultured in vitro in the presence or absence of CCL4/CCL17 (100 ng/mL) for 6 days (all HSCs were cultured in SFEM medium supplemented with 30 ng/mL SCF, 30 ng/mL TPO and 100 U/mL Penicillin–Streptomycin). (A) On the 6^{th} day, cell growth was monitored by a light microscopy, and images were acquired under an inverted microscope (Olympus CKX41). Scale bar, 500 μm. (B) The frequency of HSCs ($CD150^{+}$ $CD48^{-}$ c-KIT^{+} $SCA\text{-}1^{+}$) was analyzed on days 6 ($n = 4$).

Table S1. KEY RESOURCES TABLE

REAGENT or RESOURCE	SOURCE	IDENTIFIER
Antibodies		
Biotin Ter-119 anti-mouse (clone TER-119)	Biolegend	Cat# 116204, RRID: AB_313705
Biotin CD3ε anti-mouse (clone 145-2C11)	Biolegend	Cat# 100304, RRID: AB_312669
Biotin CD4 anti-mouse (clone RM4-5)	Biolegend	Cat# 100508, RRID: AB_312711
Biotin CD8a anti-mouse (clone 53-6.7)	Biolegend	Cat# 100704, RRID: AB_312743
Biotin CD11b anti-mouse (clone M1/70)	Biolegend	Cat# 101204, RRID: AB_312787
Biotin Ly-6G and Ly-6C anti-mouse (clone RB6-8C5)	Biolegend	Cat# 108404, RRID: AB_313369
Biotin B220 anti-mouse (clone RA3-6B2)	Biolegend	Cat# 103204, RRID: AB_312989
APC CD3ε anti-mouse (clone 145-2C11)	Biolegend	Cat# 100312, RRID: AB_312677
Alexa Fluor® 700 Gr1 anti-mouse (clone RB6-8C5)	Biolegend	Cat# 108422, RRID: AB_2137487
PerCP-Cy™5.5 CD11b anti-mouse (clone M1/70)	Biolegend	Cat# 101228, RRID: AB_893232
Pacific Blue™ B220 anti-mouse (clone RA3-6B2)	Biolegend	Cat# 103227, RRID: AB_492876
PE CD45.1 anti-mouse (clone A20)	Biolegend	Cat# 110708, RRID: AB_313497
FITC CD45.2 anti-mouse (clone 104)	Biolegend	Cat# 109806, RRID: AB_313443

Streptavidin APC-efluor780	Thermo Fisher Scientific	Cat# 47-4317-82, RRID: AB_10366688
APC CD117 anti-mouse (clone 2B8)	Thermo Fisher Scientific	Cat# 17-1171-83, RRID: AB_469431
PE-Cy™7 Sca-1 anti-mouse (clone D7)	Thermo Fisher Scientific	Cat# 25-5981-82, RRID: AB_469669
Alexa Fluor® 700 CD34 anti-mouse (clone RAM34)	Thermo Fisher Scientific	Cat# 56-0341-82, RRID: AB_493998
FITC CD34 anti-mouse (clone RAM34)	Thermo Fisher Scientific	Cat# 11-0341-85, RRID: AB_465022
PE-CF594 CD135 anti-mouse (clone A2F10.1)	BD Biosciences	Cat# 562537, RRID: AB_2737639
FITC CD16/CD32 anti-mouse (clone 2.4G2)	BD Biosciences	Cat# 553144, RRID: AB_394659
Chemicals, Peptides, and Recombinant Proteins		
Fetal Bovine Serum	GEMINI	900-108
DAPI	Sigma-Aldrich	D8417
Penicillin-Streptomycin	Gibco	15140122
D-Hanks	Solarbio	H1045
Hepes	Solarbio	H1095
PBS	Solarbio	P1022
$KHCO_3$	Sigma-Aldrich	298-14-6
NH_4Cl	Sigma-Aldrich	A9434
EDTA	Sigma-Aldrich	E6758
TRIzol	Invitrogen	15596018
Critical Commercial Assays		
PrimeScript RT reagent Kit	Takara	Cat# RR047A
PowerUp™ SYBR™ Green mix	Applied Biosystems	Cat# A25780

Mouse Cytokine Array Q4000	Raybiotech	Cat# QAM-CAA-4000-1
DNase I	NEB	Cat#M0303L
QubitTM RNA Broad Range Assay kit	Thermo Fisher	Cat# Q10210
Dispase II Dispersing enzyme II	Yeasen Biotechnology	Cat# 40104ES80
Collagenase II Collagenase type II	Yeasen Biotechnology	Cat# 40508ES76
Mouse CCL4/MIP-1β ELISA	Multisciences Biotech	Cat# EK262
Mouse CCL22/MDC ELISA Kit	Multisciences Biotech	Cat# EK2216
Human CCL17/TARC ELISA Kit	Multisciences Biotech	Cat# EK1115
Mouse CCL5/RANTES ELISA Kit	Multisciences Biotech	Cat# EK2129
Human CX3CL1/Fractalkine	Multisciences Biotech	Cat# EK1209
Mouse CCL11/Eotaxin ELISA Kit	Multisciences Biotech	Cat# EK2130
Mouse CXCL16 ELISA Kit	Multisciences Biotech	Cat# EK2254
Mouse CXCL1/KC ELISA Kit	Multisciences Biotech	Cat# EK296
Mouse TRANCE/TNFSF11/RANKL ELISA	Multisciences Biotech	Cat# EK2208
Mouse IL-22 ELISA Kit	Multisciences Biotech	Cat# EK222
Mouse IL-17B ELISA Kit	Invitrogen	Cat# EMIL17B
Mouse OPG (TNFRSF11B) ELISA Kit	Invitrogen	Cat# EMTNFRSF11B
Mouse I-TAC/CXCL11 ELISA Kit	Invitrogen	Cat# EMCXCL11
Mouse PF4 ELISA Kit	Invitrogen	Cat# EEL120
Mouse SDF-1 alpha/CXCL12 ELISA Kit	Invitrogen	Cat# EMCXCL12

Mouse LIX/CXCL5 ELISA Kit	Invitrogen	Cat# EMCXCL5
7-AAD reactive staining solution	Thermo Fisher	Cat# 00-6993-50
Xylene	Shhushi	Cat#1002341922
Anhydrous ethanol	Shhushi	Cat#100092680
Yihong dye solution	Yormbio	Cat#YM1002
Hematoxylin dye solution	Yormbio	Cat#YM1001
Hematoxylin differentiation solution	Yormbio	Cat#YM1013
Neutral gum	Sinopharm Chemical	Cat#10004160
Tartrate-Resistant Acid Phosphatase(TRAP) Stain Kit	Solarbio	Cat#G1492
Experimental Models: Organisms/Strains		
Mouse: *Dnmt3a*$^{\text{flox-R878H/+}}$	(Liao M, 2022)	N/A
Mouse: B6.Cg-*Commd10*$^{\text{Tg(Vav1-icre)A2Kio}}$/J	Jackson Laboratory	Stock# 008610
Mouse: B6.SJL-*Ptprc*$^{\text{a}}$ *Pepc*$^{\text{b}}$/BoyJ	Jackson Laboratory	Stock# 002014
Oligonucleotides		
Primers for mouse genotyping and qRT-PCR, see Table S2	Synthesized at TsingKe Biological Technology	N/A
Software and Algorithms		
GraphPad Prism 6	GraphPad Software	N/A
FlowJo™ Software	Becton, Dickinson and Company	N/A
Adobe Photoshop CS6	Adobe	N/A

Adobe Illustrator CC 2018	Adobe	N/A

Table S2 Differentially expressed genes (Top 30 upregulated genes)

R878H-LIP v.s R878H-CTL			
GeneName	logCPM	logFC	PValue
Krt78	5.01	9.10	0.00008
Krt6a	4.45	8.55	0.00050
Mir6236	5.14	5.60	0.00164
Nr4a3	5.67	2.96	0.00206
Abca12	3.23	8.77	0.00357
Nfe2l3	2.94	8.44	0.00441
Gm26760	2.63	8.16	0.00537
Ccl22	2.15	7.62	0.00537
Tns4	1.93	7.40	0.00599
Foxf1	1.54	6.81	0.00611
Csf1r	6.06	1.57	0.00612
Wmp	1.87	7.35	0.00625
5430437J10Rik	4.57	6.40	0.00634
Rnf170-ps	2.59	6.68	0.00707
Arsi	1.35	6.61	0.00746
4933402D24Rik	1.60	7.03	0.00778
2200002D01Rik	7.52	2.50	0.00779
Klrb1a	1.28	6.66	0.00860
Dcstamp	1.08	6.30	0.00922
Gm32006	4.05	4.95	0.00964
Gm29170	1.26	6.69	0.00975
Tacstd2	3.48	5.52	0.01005
Rtn2	2.57	5.16	0.01018

Psca	1.23	6.56	0.01032
Hmgb1-rs16	0.84	5.90	0.01068
Tmsb10	6.37	1.72	0.01069
Ccl4	1.76	5.70	0.01078
Klri2	1.86	6.00	0.01126
Tstd1	2.88	5.76	0.01167
Npc2	5.72	1.76	0.01172
R878H-LIP v.s WT-LIP			
GeneName	logCPM	logFC	PValue
Gsdmc2	3.00	7.78	0.00184
Cftr	1.96	6.60	0.00254
Gm49066	1.96	6.51	0.00521
Gm56667	2.69	6.34	0.00544
Gm57349	2.74	5.13	0.00584
Mgat4c	1.88	6.48	0.00605
Spaca7b	2.48	7.23	0.00640
Gm7609	2.37	7.08	0.00653
Gm42648	2.18	6.88	0.00674
Rnf43	3.87	3.16	0.00677
Gm26592	1.73	6.37	0.00721
Gm52950	1.85	6.41	0.00796
ENSMUSG00000121342	1.85	6.41	0.00796
Impg2	3.15	4.02	0.00803
Gm13162	1.65	5.94	0.00810
Muc3	2.31	5.92	0.00827
Adamts19	1.74	6.06	0.00878
Scn11a	2.89	7.71	0.00922
Phgr1	3.36	5.04	0.00925
Zg16	2.23	5.70	0.00939

A430027C01Rik	3.03	7.85	0.00963
Igkv3-12	3.21	8.02	0.00972
Ighv2-9-1	1.26	5.36	0.00997
Gm20492	0.98	4.79	0.01009
9130213A22Rik	0.98	4.79	0.01009
Il22ra2	1.36	5.50	0.01014
Gm38266	1.03	5.21	0.01144
P2rx2	3.02	7.86	0.01155
Gm12708	1.06	4.95	0.01231
Gm42421	1.07	4.97	0.01236
R878H-LIP v.s WT-CTL			
GeneName	logCPM	logFC	PValue
Qdpr	6.61	1.44	0.00182
Ccl22	3.60	6.05	0.00269
Gsdmc2	3.11	8.03	0.00286
Khk	6.44	1.36	0.00376
Xist	3.78	4.19	0.00436
F8a	3.07	7.90	0.00493
Cd209c	1.85	6.54	0.00508
Retn	2.52	6.10	0.00527
Gm34643	2.44	7.16	0.00534
Gm33732	3.04	7.87	0.00567
Mlx	6.05	1.19	0.00626
Gm37653	3.03	6.69	0.00647
Gm10522	1.83	6.41	0.00647
Babam1	5.73	1.35	0.00663
Chrna9	2.59	7.39	0.00720
Tstd1	1.76	5.33	0.00727
Phgr1	3.46	5.81	0.00766

Igkv3-4	2.73	7.59	0.00857
Gm13162	1.69	6.22	0.00885
Gm42648	2.24	7.13	0.00901
Gm48583	1.67	6.41	0.00907
Fcgbp	3.88	4.79	0.00918
Cidea	2.70	4.74	0.00948
H2-Q10	8.45	1.13	0.00949
Spaca7b	2.56	7.48	0.00953
Htr7	1.27	5.62	0.00975
Gm34189	1.23	5.53	0.00976
4930414N06Rik	2.53	4.90	0.01077
Wmp	1.79	6.64	0.01124
Gm18807	1.55	6.11	0.01142

Table S3 Cytokine array results

(pg/ml)	WT-CTL-PB	WT-LIP-PB	R878H-CTL-PB	R878H-LIP-PB	LOD	MAX
AR	*0.0*	10.6	3.2	30.5	3.0	2,000.0
Axl	882.3	402.4	685.2	918.0	8.4	10,000.0
CD27L	31.6	26.0	*18.2*	*5.2*	22.0	6,666.7
CD30	54.1	54.9	38.6	50.2	9.0	10,000.0
CD40	3.8	11.7	7.5	7.4	3.0	1,111.1
CXCL16	16.3	59.1	82.6	88.2	0.3	1,000.0
EGF	1,524.2	387.9	136.6	**2,075.1**	0.9	2,000.0
E-selectin	**4,938.7**	**4,250.5**	**5,648.4**	**5,450.9**	2.6	4,000.0
Fractalkine	3,865.7	1,445.6	1,562.4	5,497.0	14.7	100,000.0
GITR	7.6	2.3	4.9	5.3	2.1	4,000.0
HGF	1,207.3	1,803.5	2,969.0	6,168.8	83.8	20,000.0
IGFBP-2	23,022.1	21,449.1	24,211.3	31,418.6	135.8	100,000.0
IGFBP-3	14,020.8	15,576.3	15,527.6	15,044.4	23.0	20,000.0
IGFBP-5	1,236.4	1,202.1	1,582.3	9,378.7	28.0	13,333.3
IGFBP-6	17,983.8	28,350.9	24,158.8	30,036.2	23.6	40,000.0
IGF-1	8,407.9	9,961.4	9,301.2	8,271.8	2.1	10,000.0
IL-12p70	*0.0*	9.2	*0.0*	*5.0*	5.7	4,000.0
IL-17E	101.6	125.8	93.0	53.8	26.9	40,000.0

IL-17F	*0.0*	*41.4*	*0.0*	143.7	107.4	40,000.0
IL-1ra	66.6	147.2	139.0	1,520.8	11.1	4,000.0
IL-2 Ra	560.3	570.1	584.7	1,445.9	10.2	10,000.0
IL-20	56.2	*15.4*	63.2	45.5	40.4	20,000.0
IL-23	*0.0*	49.9	*0.0*	*0.0*	44.1	4,444.4
IL-28	*0.9*	*1.0*	8.1	*0.0*	2.6	2,000.0
I-TAC	*0.0*	*0.0*	*0.0*	1,627.9	28.4	20,000.0
MDC	83.3	76.3	92.0	83.2	0.6	1,000.0
MIP-2	2.4	3.2	1.0	0.8	0.6	1,000.0
MIP-3a	101.4	41.7	40.6	74.9	0.8	1,000.0
OPN	13,713.1	16,188.6	17,512.9	**20,612.0**	36.8	20,000.0
OPG	527.3	212.7	422.8	815.2	8.3	2,222.2
Prolactin	374.0	557.1	403.8	**2,531.8**	8.5	1,111.1
Pro-MMP-9	44,380.6	54,553.1	57,234.7	40,887.6	16.6	100,000.0
P-selectin	**2,951.1**	**3,353.2**	**2,784.1**	**2,970.9**	8.2	1,333.3
Resistin	570.4	486.1	545.8	308.2	2.5	666.7
SCF	*4.2*	45.0	75.0	3,029.1	17.3	10,000.0
SDF-1a	759.8	770.0	805.7	1,118.2	42.1	100,000.0
THPO	*55.6*	386.3	235.4	160.3	153.4	33,333.3
VCAM-1	**4,253.7**	**4,303.7**	**4,474.4**	3,991.5	2.6	4,000.0
VEGF	48.3	105.1	61.8	564.8	4.4	4,000.0
VEGF-D	*0.0*	2.8	*1.1*	*0.8*	1.2	4,000.0
4-1BB	2,168.3	1,895.7	2,402.8	2,297.8	129.8	25,000.0
ACE	**121,981.5**	**109,048.1**	**139,910.3**	**202,897.0**	161.5	100,000.0
ALK-1	103.6	58.8	81.2	1,865.7	9.0	10,000.0
CT-1	75.5	*0.0*	77.1	104.2	38.7	40,000.0
CD27	*0.0*	56.7	*0.0*	*0.0*	20.0	25,000.0
CD40L	2,724.0	2,817.6	3,114.1	36,923.4	19.6	40,000.0
CTLA4	5.1	6.2	8.9	250.4	0.3	2,500.0
Decorin	2,929.3	4,861.3	3,425.2	**7,797.1**	1.1	5,000.0
Dkk-1	11,188.3	10,879.4	10,125.1	22,840.0	19.9	40,000.0
Dtk	33.9	20.0	76.9	41.3	4.9	20,000.0
Endoglin	478.0	392.8	462.1	504.5	6.4	10,000.0
Fcg RIIB	1,722.7	1,593.4	1,774.7	2,006.3	0.9	10,000.0
Flt-3L	788.2	816.2	749.7	901.9	0.8	25,000.0
Galectin-1	2,159.1	4,680.4	3,320.2	**14,003.0**	6.5	10,000.0
Galectin-3	623.0	649.8	669.9	741.6	0.4	2,000.0
Gas 1	774.9	775.7	768.2	1,918.3	1.7	2,000.0
Gas 6	2,138.0	2,335.8	2,418.3	**3,658.7**	0.5	2,500.0
GITR L	57.8	35.2	52.3	123.9	0.4	1,000.0
HAI-1	48.2	68.8	76.9	149.2	9.1	10,000.0
HGF R	177.0	527.7	131.1	244.9	20.4	25,000.0
IL-1 R4	714.4	655.8	528.2	823.3	11.3	40,000.0

IL-3 Rb	1,322.8	2,192.5	2,846.4	3,615.4	76.1	40,000.0
IL-9	50.4	92.2	49.4	49.7	3.0	20,000.0
JAM-A	2,798.8	2,445.1	2,519.5	**5,290.2**	2.3	5,000.0
Leptin R	238.5	314.7	301.9	301.5	6.4	5,000.0
L-Selectin	9,088.7	8,793.7	8,054.0	9,319.3	1.1	10,000.0
Lymphotactin	938.8	1,018.9	1,853.6	1,312.9	67.3	200,000.0
MadCAM-1	216.4	198.7	249.9	332.1	0.6	1,111.1
MFG-E8	144.8	393.9	198.7	351.4	2.6	13,333.3
MIP-3b	*0.0*	*0.0*	*0.0*	*0.0*	0.6	1,000.0
Neprilysin	649.0	632.3	857.2	6,988.9	15.0	20,000.0
Pentraxin 3	6,692.1	9,323.2	6,366.6	7,834.5	8.3	10,000.0
RAGE	*4.9*	33.9	15.1	*2.7*	8.6	25,000.0
TACI	203.2	240.7	302.4	309.5	9.5	50,000.0
TREM-1	125.2	173.6	157.9	2,731.1	7.7	10,000.0
TROY	63.2	93.6	48.2	886.9	6.2	4,000.0
TSLP	0.6	5.4	3.1	2.0	0.4	4,000.0
TWEAK R	22,668.4	**31,101.7**	**27,038.6**	**72,055.6**	10.9	25,000.0
VEGF R1	768.1	1,039.8	1,049.5	**11,118.5**	12.4	10,000.0
VEGF R3	107.8	142.3	128.8	156.8	7.2	10,000.0
bFGF	*0.0*	*0.0*	*0.0*	*0.0*	2.8	5,000.0
BLC	*0.0*	*0.0*	*0.0*	92.2	28.3	10,000.0
CD30L	*0.0*	*0.0*	*0.0*	*0.0*	0.9	2,000.0
Eotaxin	157.9	215.7	274.9	382.3	0.4	1,000.0
Eotaxin-2	*0.0*	*0.0*	*0.0*	*0.0*	2.6	1,000.0
Fas L	*0.0*	*0.0*	*0.0*	*0.0*	14.8	10,000.0
G-CSF	738.5	365.0	1,242.0	1,143.3	40.0	20,000.0
GM-CSF	*0.0*	*0.0*	*0.0*	*0.0*	5.4	10,000.0
ICAM-1	1,640.5	1,198.3	116.7	4,074.3	14.1	10,000.0
IFNg	*0.0*	*0.0*	*0.0*	*0.0*	12.0	4,000.0
IL-1a	8.9	*0.0*	*0.0*	4.0	1.2	2,000.0
IL-1b	*0.0*	*0.0*	*0.0*	*0.0*	7.9	4,000.0
IL-2	*0.0*	*0.0*	*0.0*	*0.0*	4.6	10,000.0
IL-3	4.5	0.7	6.6	*0.0*	0.3	2,000.0
IL-4	*0.0*	*0.0*	*0.0*	*0.0*	0.6	166.7
IL-5	*0.0*	*0.0*	*0.0*	*0.0*	27.3	10,000.0
IL-6	*0.0*	*0.0*	*0.0*	*0.0*	6.3	1,333.3
IL-7	*0.0*	*0.0*	*0.0*	70.6	12.4	1,111.1
IL-10	*0.0*	*0.0*	*0.0*	*0.0*	24.7	10,000.0
IL-12p40	*0.0*	*0.0*	*0.0*	*0.0*	5.5	1,000.0
IL-13	*0.0*	*0.0*	*0.0*	*0.0*	15.0	20,000.0
IL-15	*0.0*	*0.0*	*0.0*	*0.0*	47.5	100,000.0
IL-17	*0.0*	*0.0*	*0.0*	*0.0*	1.1	4,000.0
IL-21	2,922.8	1,900.5	2,726.3	1,720.2	56.5	20,000.0

KC	119.7	164.7	127.5	106.7	0.5	2,000.0
Leptin	1,610.4	2,833.4	6,859.7	*0.0*	57.1	100,000.0
LIX	1,301.0	1,070.8	3,061.2	2,749.4	13.2	20,000.0
MCP-1	*0.0*	*0.0*	*0.0*	*0.0*	3.4	4,000.0
MCP-5	23.4	5.2	3.5	*0.0*	0.6	1,000.0
MCSF	*0.0*	*0.0*	25.8	*0.0*	1.1	2,000.0
MIG	*0.0*	39.9	*0.0*	677.1	13.2	10,000.0
MIP-1a	*0.0*	*0.0*	*0.0*	*0.0*	2.1	10,000.0
MIP-1g	871.9	845.9	938.7	**1,217.7**	0.7	1,000.0
PF4	8,105.8	8,225.4	6,944.8	9,747.3	7.1	20,000.0
RANTES	*0.0*	*0.0*	*0.0*	26.9	1.2	4,000.0
TARC	*0.0*	6.8	*0.0*	34.6	1.6	4,000.0
TCA-3	*0.0*	*0.0*	*0.0*	10.6	0.9	2,000.0
TNF RI	208.1	225.4	212.6	299.0	0.2	500.0
TNF RII	672.7	694.7	700.4	930.3	0.6	2,000.0
TNFa	*0.0*	*0.0*	*0.0*	*0.0*	3.2	1,000.0
6Ckine	142.8	*1.1*	*19.2*	65.2	31.5	20,000.0
Activin A	9.7	*1.7*	13.7	3.6	2.1	4,000.0
ADAMTS1	549.6	341.0	360.6	10,682.6	26.2	13,333.3
Adiponectin	**6,062.9**	**5,314.8**	**6,933.7**	**5,939.8**	11.8	3,333.3
ANG-3	409.9	110.0	518.7	375.0	24.4	40,000.0
ANGPTL3	15,004.4	15,263.3	22,171.7	16,533.9	63.4	100,000.0
Artemin	20.8	*0.4*	14.5	8.8	0.9	4,000.0
CCL28	312.6	*0.0*	*0.0*	*0.0*	64.9	100,000.0
CD36	7,671.8	7,749.3	11,999.4	91,913.7	199.6	200,000.0
Chordin	771.3	303.8	412.9	2,248.6	10.9	3,333.3
CRP	3,600.1	3,008.2	**4,150.1**	3,750.1	6.4	4,000.0
E-Cadherin	2,120.7	1,710.5	2,157.1	1,857.3	2.5	10,000.0
Epigen	630.2	426.4	726.3	582.6	24.0	20,000.0
Epiregulin	2,603.2	790.5	2,630.6	3,487.2	205.4	200,000.0
Fas	104.0	45.6	128.7	215.9	16.3	10,000.0
Galectin-7	733.3	485.7	742.8	158.2	110.6	100,000.0
gp130	2,857.4	1,329.2	3,728.2	3,316.6	24.9	10,000.0
Granzyme B	435.0	243.9	294.4	6,656.0	16.4	6,666.7
Gremlin	1,550.0	265.5	1,287.2	819.2	79.6	100,000.0
IFNg R1	6.5	*0.7*	*2.1*	*0.0*	3.1	2,000.0
IL-17B	586.3	198.5	1,005.1	20,646.8	142.1	200,000.0
IL-17B R	*12.4*	*117.1*	1,270.8	227.6	201.2	100,000.0
IL-22	1,185.6	826.2	1,479.1	12,585.8	70.7	13,333.3
MIP-1b	28.4	3.5	9.6	10.4	1.3	4,000.0
MMP-2	11,992.9	10,984.3	19,578.6	18,775.5	28.8	20,000.0
MMP-3	8,033.2	6,784.4	7,989.0	7,830.7	3.8	10,000.0
MMP-10	12.5	2.6	7.8	8.5	0.4	1,000.0

PDGF-AA	892.5	726.1	1,081.1	800.1	1.6	1,333.3
Persephin	11.1	8.1	10.4	8.1	0.6	4,000.0
sFRP-3	93.7	5.9	69.7	56.2	5.2	20,000.0
Shh-N	12.6	*0.0*	*2.1*	*0.0*	5.6	3,333.3
SLAM	78.0	378.0	141.0	348.4	70.1	100,000.0
TCK-1	93,009.0	83,874.3	123,806.8	85,798.8	42.5	200,000.0
TECK	365.9	301.9	171.0	62.2	59.9	200,000.0
TGFb1	1,414.0	1,265.5	2,282.6	1,382.2	71.2	100,000.0
TRANCE	1,770.8	718.6	631.1	17,859.5	78.2	40,000.0
TremL1	13,327.3	11,076.1	**14,703.2**	11,542.6	32.6	13,333.3
TWEAK	164.6	130.6	250.1	121.4	29.1	20,000.0
VEGF-B	*23.0*	*0.0*	*0.0*	*0.0*	24.7	10,000.0
VEGF R2	58.6	6.3	8.3	26.8	4.4	3,333.3
B7-1	3,384.8	3,903.9	3,360.3	**4,793.2**	7.4	4,000.0
BAFF R	387.1	342.4	323.8	531.1	2.4	1,000.0
BTC	51.3	41.4	58.1	64.6	2.3	2,000.0
C5a	720.0	807.6	786.3	805.4	0.8	1,000.0
CCL6	566.4	1,184.6	711.9	721.4	9.4	40,000.0
CD48	**2,164.5**	**2,573.9**	**2,130.4**	**4,822.9**	2.2	2,000.0
CD6	36.5	64.9	48.6	81.1	1.0	1,000.0
Chemerin	69,365.5	88,639.5	74,607.8	72,839.5	106.3	100,000.0
Clusterin	7,640.1	7,710.5	7,444.3	45,235.9	85.3	100,000.0
Lungkine	*0.0*	*50.3*	*0.0*	879.7	277.1	200,000.0
Cystatin C	**1,481.3**	**1,687.7**	**1,537.6**	**4,554.0**	3.2	666.7
DAN	1,528.4	1,649.6	1,516.9	1,667.4	13.5	100,000.0
DLL4	958.2	2,131.4	2,595.0	3,115.0	145.0	40,000.0
EDAR	5,778.5	6,684.6	6,671.0	6,585.0	21.1	20,000.0
Endocan	5,596.6	5,551.5	6,018.2	6,086.0	13.1	20,000.0
Fetuin A	**134,823.0**	**133,527.2**	**131,583.7**	**157,207.9**	190.4	100,000.0
H60	124.9	88.4	127.6	139.7	3.1	2,000.0
IL-33	15.7	9.9	16.9	1,398.0	1.5	4,000.0
IL-7 Ra	14,490.4	9,562.5	12,973.4	14,758.3	90.6	40,000.0
Kremen-1	191.3	229.2	249.0	342.1	10.4	4,000.0
Limitin	122.1	78.4	105.2	112.2	2.4	1,000.0
Lipocalin-2	54,198.4	61,774.3	53,124.7	42,456.1	6.3	100,000.0
LOX-1	382.9	866.7	1,091.9	1,237.8	14.4	4,000.0
Marapsin	*1.5*	90.1	102.9	*0.0*	37.5	20,000.0
MBL-2	**4,602.0**	**5,192.6**	**4,962.1**	**6,058.8**	0.9	2,000.0
Meteorin	*0.0*	153.3	186.0	244.2	26.3	40,000.0
Nope	3,754.7	4,779.6	4,908.4	**19,822.0**	19.5	10,000.0
NOV	6,602.4	7,458.6	7,598.5	7,196.5	8.1	40,000.0
Osteoactivin	619.5	1,287.4	747.4	8,271.2	17.6	10,000.0
OX40 Ligand	1,028.7	1,273.7	1,020.8	1,044.3	4.8	4,000.0

P-Cadherin	633.7	863.6	552.2	**5,728.4**	8.6	4,000.0
Periostin	**20,331.4**	**18,181.3**	**19,756.3**	**26,047.7**	8.7	4,000.0
PlGF-2	149.7	122.2	147.7	149.6	1.0	1,000.0
Progranulin	49,559.4	26,607.8	51,087.9	30,610.2	23.6	100,000.0
Prostasin	18,356.6	20,444.7	17,711.0	48,397.6	34.9	100,000.0
Renin 1	**41,238.9**	**45,746.1**	**40,759.8**	**94,485.0**	80.1	40,000.0
Testican 3	2,771.0	2,393.5	2,803.9	3,139.5	18.8	40,000.0
TIM-1	13,494.8	16,059.8	12,709.6	14,734.0	102.8	100,000.0
TRAIL	*0.0*	94.6	51.6	64.9	12.6	10,000.0
Tryptase e	9,523.5	11,167.4	11,117.5	11,516.4	36.6	100,000.0